

AFIT/GSO/ENY/93D-6

3 AD-A273 824



SHIELDED COIL ELECTRODYNAMIC PROPULSION  
(SCEP)

A FEASIBILITY STUDY

THESIS

Richard J.R. Ladouceur  
Major, CAF

AFIT/GSO/ENY/93D-6

DTIC  
ELECTE  
DEC 16 1993  
S E D

93-30474



Approved for public release; distribution unlimited

93 12 15 08 2

SHIELDED COIL ELECTRODYNAMIC PROPULSION (SCEP)  
A FEASIBILITY STUDY

THESIS

Presented to the Faculty of the Graduate School of Engineering  
of the Air Force Institute of Technology  
Air University  
In Partial Fulfillment of the  
Requirements for the Degree of  
Master of Science in Space Operations

Richard J.R. Ladouceur, B.S.  
Major, CAF

December 1993

Accession For	
NTIS	CRA&I <input checked="" type="checkbox"/>
DTIC	TAB <input checked="" type="checkbox"/>
Unannounced <input type="checkbox"/>	
Justification _____	
By _____	
Distribution / _____	
Availability Codes	
Dist	Avail and/or Special
A-1	

Approved for public release; distribution unlimited

DTIC QUALITY INSPECTED 1

### Acknowledgements

I thank my thesis advisor, Dr. Curtis Spenny, for his patience and support. Most of all I sincerely thank him for keeping an open mind throughout this research effort. I thank my committee members Dr. W. Bailey, Dr. V. Pyati, and Maj. Burke for their assistance in their fields of expertise, and for the time and genuine concern which they have displayed through the quality and pertinence of their recommendations throughout the project. Also, I thank the technicians of the ENY department for their support which allowed for the completion of the experiment on time. This effort is dedicated to my dear wife Lisa for her exceptional support.

Richard J.R. Ladouceur

## Table of Contents

List of Figures . . . . .	vii
List of Table . . . . .	ix
Abstract . . . . .	x
I. Introduction . . . . .	1-1
1.1 Electrodynamic Propulsion - Shielded Coil . . .	1-4
1.1.1 An Example . . . . .	1-6
1.2 Magnetic Shield . . . . .	1-7
1.3 Magnetic Field - Terminology . . . . .	1-8
1.4 Report Outline . . . . .	1-8
II. Shielding a Magnetic Force . . . . .	2-1
2.1 Ferromagnetism . . . . .	2-1
2.1.1 Introduction . . . . .	2-1
2.1.2 Magnetic Field Intensity ( $H$ ) vs Magnetic Field Density ( $B$ ) . . . . .	2-2
2.1.3 Magnetization . . . . .	2-3
2.1.4 B&H Curve - Relative Permeability $\mu_r$ . . .	2-6
2.1.5 Initial Magnetization . . . . .	2-7
2.1.6 B&H - Hysteresis . . . . .	2-8
2.2 High Permeability Material . . . . .	2-10
2.2.1 Boundary Effect . . . . .	2-10

2.3	Magnetic Field Around Magnetic Shield . . . . .	2-14
2.3.1	Introduction . . . . .	2-14
2.3.2	Magnetic Shield - External triggering Field . . . . .	2-14
2.3.3	Magnetic Shield - Internal Triggering Field . . . . .	2-18
2.3.4	Combining the fields . . . . .	2-19
2.4	Summary . . . . .	2-20
III.	Shielding Effectiveness . . . . .	3-1
3.1	Introduction . . . . .	3-1
3.1.1	Shielding Factor . . . . .	3-1
3.1.2	Cylindrical Geometry . . . . .	3-2
3.1.3	End Effects . . . . .	3-3
3.1.4	Applied Magnetic Field - Vector Notation	3-4
3.2	Residual External Triggering Field . . . . .	3-4
3.2.1	Introduction . . . . .	3-5
3.2.2	Shield Efficiency - External triggering Field . . . . .	3-6
3.2.3	Applied Magnetic Field Density - External triggering Field . . . . .	3-7
3.2.4	Applied Magnetic Field Density - Internal Field . . . . .	3-8
3.2.5	Applied Magnetic Field Density - Total .	3-9
3.2.6.	An Example . . . . .	3-10
3.3	Magnetic Surface Current Density - $H_{\text{etf}}$ . . . . .	3-12
3.3.1	Estimating $J_{\text{sm-etf}}$ . . . . .	3-12

3.3.2	An Example . . . . .	3-14
3.4	Magnetic Surface Current Density - $H_{\text{surf}}$ . . . . .	3-15
3.4.1	Estimating Current . . . . .	3-15
3.4.2	An Example . . . . .	3-16
3.5	SCEP Performance . . . . .	3-16
3.5.1	An Application . . . . .	3-17
3.6	Shield Shaking . . . . .	3-19
3.6.1	Shield's Magnetization . . . . .	3-19
3.6.2	Shaking Coil . . . . .	3-21
3.7	Summary . . . . .	3-22
IV.	Experimental Demonstration . . . . .	4-1
4.1	Introduction . . . . .	4-1
4.1.1	Aim . . . . .	4-1
4.1.2	The Space Environment . . . . .	4-1
4.2	Design Considerations . . . . .	4-2
4.2.1	Induced Magnetic Force . . . . .	4-2
4.2.2	Coil and Torque . . . . .	4-2
4.2.3	Torque vs Force . . . . .	4-3
4.2.4	Generating a Magnetic Field . . . . .	4-3
4.2.5	Measurements . . . . .	4-5
4.2.6	Static Imbalance . . . . .	4-9
4.2.7	Test Setup . . . . .	4-11
4.2.8	Limitation . . . . .	4-14
4.3	Test Procedure . . . . .	4-15
4.3.1	Unshielded Loop . . . . .	4-15
4.3.2	Shielded Loop . . . . .	4-16

4.3.3	Manual Shaking Procedure . . . . .	4-17
4.4	Results . . . . .	4-17
4.5	Conclusion . . . . .	4-19
V.	Conclusions and Recommendations . . . . .	5-1
5.1	Conclusions . . . . .	5-1
5.2	Recommendations . . . . .	5-3
5.2.1	Additional Validation - Model . . . . .	5-4
5.2.2	Application Considerations . . . . .	5-4
Appendix A: Magnetic Field - Internal Triggering Field . .		A-1
Bibliography . . . . .		Bib-1

### List of Figures

Figure 1.	Space propulsion technology tree. . . . .	1-3
Figure 2.	Unshielded loop exposed to earth's magnetic field. . . . .	1-5
Figure 3.	Shielded loop exposed to the earth's magnetic field. . . . .	1-6
Figure 4.	Electron's spin submitted to external triggering field (Johnk, 1975:152). . . . .	2-2
Figure 5.	Magnetization field within magnetized iron rod (Johnk, 1975:1522). . . . .	2-4
Figure 6.	Surface magnetic current density. . . . .	2-5
Figure 7.	Initial magnetization curve. (Krauss J. D., 1984:242) . . . . .	2-7
Figure 8.	Hysteresis effect. (Krauss J. D., 1984:246) . . . . .	2-8
Figure 9.	Wall motion regions. (Johnk C.T.A., 1975:153) . . . . .	2-11
Figure 10.	Boundary conditions: a conductor in vacuum (left); conductor in high permeability material (right). (Van Bladel J., 1964:177) . . . . .	2-13
Figure 11.	Conceptual illustration of the external and induced fields in and around a cylindrical shield. . . . .	2-16
Figure 12.	Equation derived field in and around a cylindrical shield for $\mu_r = 50$ . (Rikitake T., 1990:1232) . . . . .	2-17



Figure 13.	Conceptual illustration of the combined fields within a cylindrical shield. . . . .	2-20
Figure 14.	Cylindrical shield nomenclature. . . . .	3-3
Figure 15.	Cylindrical shield efficiency vs length/diameter (Mager,1970:68). . . . .	3-4
Figure 16.	Shaking coil wrapped around a cylindrical shield. . . . .	3-21
Figure 17.	Demagnetization process. . . . .	3-23
Figure 18.	Field generation by a pair of Helmholtz coils. . . . .	4-5
Figure 19.	Center coil placement in the magnetic field. . . . .	4-6
Figure 20.	Angle indicator relative position. . . . .	4-8
Figure 21.	Definition of $\theta_f$ and $\theta_{rot}$ . . . . .	4-10
Figure 22.	Center coil mass distribution. . . . .	4-11
Figure 23.	Balancing the center coil. . . . .	4-12
Figure 24.	Concentrator. . . . .	5-5
Figure 25.	Cylindrical coordinate reference system. . . .	A-1

### List of Table

Table I.	Performance Parameters. . . . .	1-2
Table II.	Incident vs transmitted angle with $\mu_r =$ 30,000. . . . .	2-12
Table III.	SCEP Performance Potential. . . . .	3-20
Table IV.	Test hardware specifications. . . . .	4-13
Table V.	Measurements. . . . .	4-18

Abstract

This study investigated Shielded Coil Electrodynamic Propulsion (SCEP). The use of the earth's magnetic field as a propulsion source has been previously investigated. The non-uniformity of the earth's magnetic field at the pole has been considered as a potential region for the application of field differential propulsion. This concept of propulsion is limited to inclinations near the magnetic poles where a current loop may be exposed to a non-uniform field. Also, the concept of conductor segments structurally attached to a spacecraft and closing through the ionosphere (POTkV) has been investigated. It was found that a significant amount of power and long conductors were required in order for a POTkV to complete its assigned tasks. A more compact propulsion concept which requires significantly less power is proposed. This concept relies on the feasibility of significantly reducing the magnetic force induced by the earth's magnetic field on selected segments of a coil. Accordingly, this study primarily focuses on the magnetic shield and its ability to reduce the induced magnetic force on a shielded conductor and the shield itself. The properties of high permeability ferromagnetic material were reviewed. This indicated that in the presence of a magnetic shield, the induced magnetic force would be significantly reduced. To support the theoretical model an experiment was conducted. The experiment consisted of exposing a coil to a magnetic field. The rotation induced on the coil was reduced by a factor of 80 when the

coil was shielded. Finally, a brief calculation of the SCEP performance suggest that it has significant potential for space applications. Therefore, the findings of this study make the SCEP a valuable propulsion concept.

# SHIELDED COIL ELECTRODYNAMIC PROPULSION (SCEP)

## - A FEASIBILITY STUDY

### I. Introduction

Space propulsion systems have been developed to accomplish the different tasks associated with space operations. Chemical propulsion is predominantly used for tasks which require significant thrust. For example, the space shuttle uses 38 thrusters each capable of producing 3870 (N) (Sutton, G.P., 1992:16) for small vehicle velocity adjustments and attitude control. A chemical rocket's thrust is not easily modulated, so chemical rockets have limited capability for tasks associated with precise maneuvering such as docking. Nuclear rockets are also a high thrust engine, however, current interest in this propulsion system lies in its potential to achieve manned planetary missions. Electric propulsion is designed to achieve tasks which require low to moderate thrust for an extended period of time. This type of propulsion is characterized by its high specific impulse compared to chemical propulsion. Table I provides some performance parameters for various types of propulsion systems. Finally, the use of the earth's magnetic field as a propulsion source created a new type of propulsion system which for the purpose of this report is referred to as "field propulsion". Figure 1 is a tree representing the interrelation amongst the different propulsion systems.

Table I. Performance Parameters.

Type	Thrust Range (mN)	Specific Impulse (sec)	Thrust Duration
Resistojet (thermal)	2-100	200-300	months
Arcjet (thermal)	2-700	400-1500	months
Ion	0.001-200	1500-5000	months
Solid pulsed plasma	0.05-10	1000-2000	years
MPD*	0.001-2000	1000-8000	months
Monopropellant rocket	30-100,000	200-230	hours or minutes

\*MPD: Magneto Plasma Dynamic

In 1965 Drell, Foley, and Ruderman proposed that the earth's magnetic field may be used to provide a propulsive force to a spacecraft (Drell, and others, 1965). This concept inspired the design of the electrodynamic tethers which have a number of non-electrodynamic applications (Penzo and Ammann, 1989:120). Accordingly, an electrically conducting tether can be used for propulsion. This means that when a current circulates in the tether, the earth's magnetic field will induce a magnetic force on the tether.

The possibility of using an electrodynamic force resulting from the interaction of the earth's magnetic field with a current carrying conductor to precisely follow other space vehicles at close range, dock with other spacecraft, and perform gross orbital

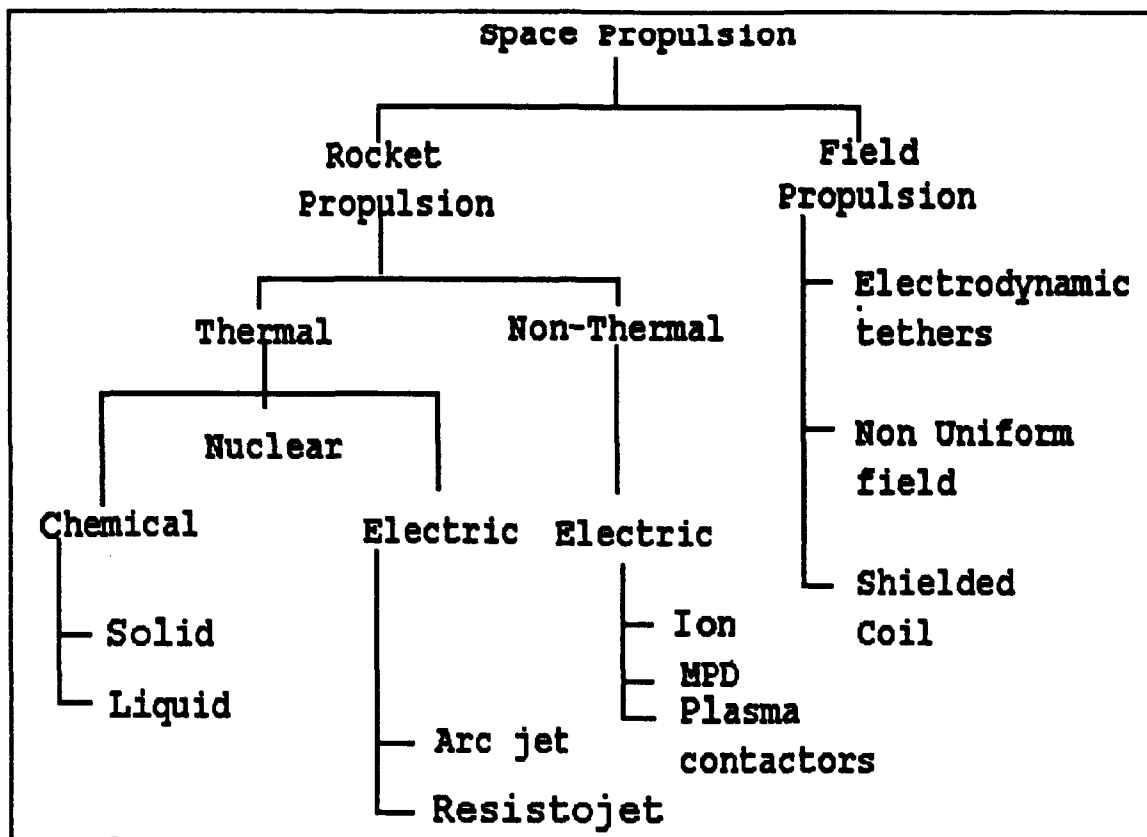


Figure 1. Space propulsion technology tree.

maneuver has been investigated (Spenny and Lawrence, 1993). In particular, their research centered on using multiple segments of conducting wire structurally attached to a satellite to provide thrust and attitude control. The ambient plasma in the ionosphere is used to close the current path between one end of the conductor and the other (Penzo and Ammann, 1989:120). Plasma contactors at either end of the wire segment are used to promote this current flow. The process of connecting and closing the loop through the ionosphere increases the resistance of the total circuit. While the actual magnitude of this resistance is not known precisely, it is estimated to be between one and twenty ohms (Penzo and Ammann, 1989:125). Two of the findings for such a system are:

1. that in order to accomplish the assigned task the power requirement is significantly large; and
2. that the length of the conductor needed is relatively long - 620 to 1700 meters (Lawrence, R. Jr. 1992:5-8).

The non-uniformity of the earth's magnetic field near the magnetic pole has been proposed as a source of propulsion (Engelberger, 1970). This type of propulsion is referred to as differential field propulsion. Essentially, a current loop exposed to a non-uniform magnetic field will experience a net force. Accordingly, Engelberger suggests that near the magnetic pole where the earth's magnetic field is less uniform, a spacecraft attached to a large enough loop would experience sufficient force to propel itself. Differential field propulsion is limited to regions where the magnetic field varies in magnitude and/or direction, so, this type of propulsion is limited to high inclination orbits.

In order to reduce the power requirement, reduce the length of the conductor, and maintain the ability to operate in any inclination orbit, this thesis investigates the feasibility of using a partly shielded closed loop multiple-turn conductor wire in lieu of a conductor segment with plasma contactors.

### 1.1 Electrodynamic Propulsion - Shielded Coil

Electromagnetic theory indicates that a current loop subjected to a uniform magnetic field will experience a torque. The force induced on a current element  $d\mathbf{L}$  due to a magnetic flux density  $\mathbf{B}$  is given by (Herbert and Neff, 1987:195):



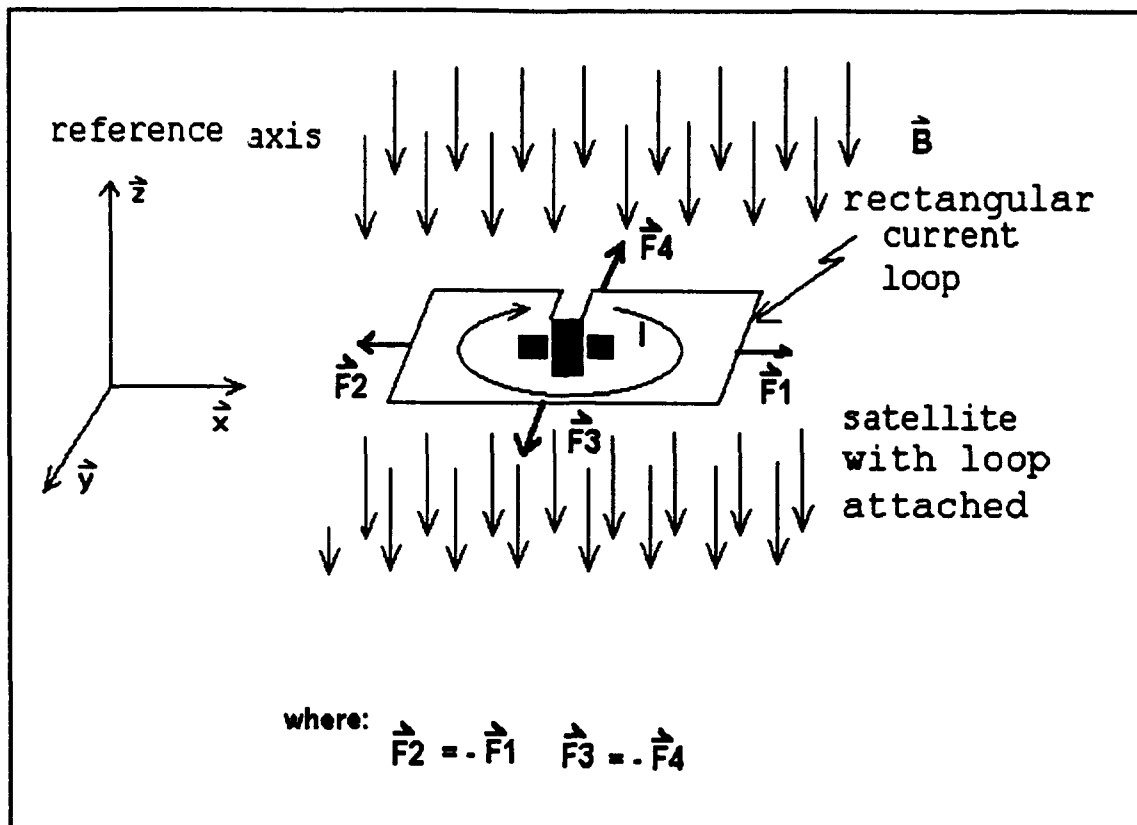


Figure 2. Unshielded loop exposed to earth's magnetic field.

$$d\vec{E} = I d\vec{L} \times \vec{B} \quad (1)$$

Consider a rectangular loop exposed to a magnetic flux density constant in direction and magnitude. Equation (1) may then be integrated over each segment of the loop to obtain the force:

$$\begin{aligned} \underline{F}_i &= I \underline{L}_i \times \vec{B} \\ \forall i &= 1,2,3,4 \end{aligned} \quad (2)$$

Figure 2 illustrates how the force will act on each segment of the loop. Now, consider a rectangular loop with three of its segments

shielded such that the force may only arise on one segment. Therefore, as seen in Figure 3, the loop will experience a net force in lieu of a torque. This new propulsion concept is named Shielded Coil Electrodynamic Propulsion (SCEP), and it essentially relies on the ability to prevent the earth's magnetic field from inducing a magnetic force upon the shield and the shielded segments of the loop.

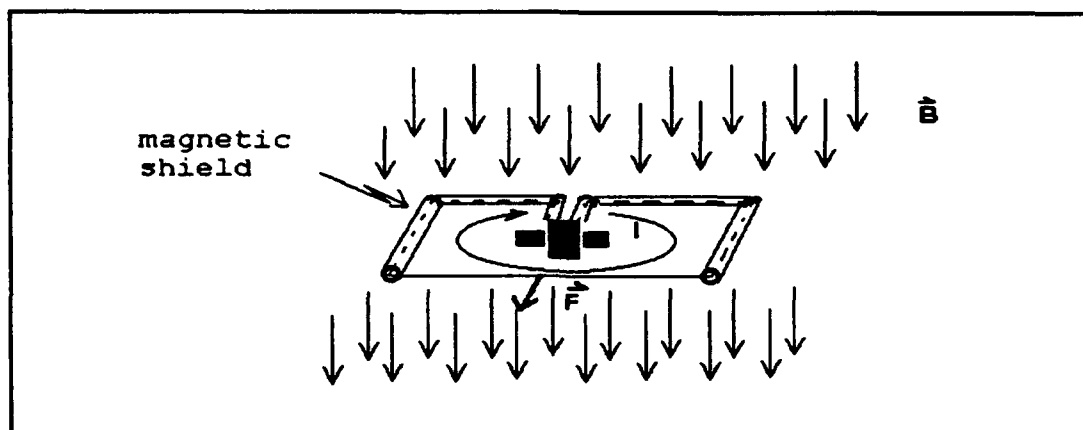


Figure 3. Shielded loop exposed to the earth's magnetic field.

A partly shielded coil offers many advantages. First, a closed loop circuit, such as a coil, does not have to use the ionosphere as a current return path, thereby reducing the resistance of the circuit to that of the resistance of the conductor wire of the coil.

1.1.1 An Example. Consider, a 1 (km) aluminum wire is required in order to replace the plasma contactors and close the loop. Since the current may be of the order of 1000 (amps), the conductor wire diameter will be 4 (cm). The resistivity of an aluminum wire is  $2.8 \times 10^{-8}$  (ohm\*m), therefore, the resistance of the

wire will be 0.022 (ohm). Assuming a resistance of 1 (ohm) for the ionosphere, the circuit resistance will be reduced by a factor of slightly greater than 40.

Secondly, a coil is constructed with a number of turns wrapped one on top of the other, thereby allowing for a much more compact design. The 1 (km) long by 4 (cm) diameter tether discussed in example 1.1.1 could be replaced by a 1 (m) X 0.25 (m) rectangular coil of 1000 turns in which a 1 (amp) current circulates. The 4 (cm) diameter conductor wire would then be replaced by a 0.05 (cm) conductor wire. Finally, a high amplitude pulsed current may be used in the partly shielded closed loop circuit. This is advantageous since a more efficient power source such as capacitor could be used to generate the current required to obtain thrust.

## 1.2 Magnetic Shield

In the SCEP application, it is anticipated that a cylindrical magnetic shield will be wrapped around those segments of the loop for which it will be undesirable that the earth's magnetic field induce a force. Since magnetic shields are currently used to prevent a magnetic field from entering (Baum and Bork, 1991:69) or leaving (Haga and Nasuno, 1990:759) a given region, it is expected that the cylindrical shield will effectively reduce the magnetic force due to the earth's magnetic field on the shielded conductor. However, the SCEP application capitalizes on the ability to prevent the earth's magnetic field from inducing a magnetic force upon the shield as well as the shielded conductor.

Therefore, this feasibility study will primarily focus on the

quantitative definition of the residual magnetic forces induced on the shielded conductor and the shielding material for the particular case of a shield submitted to the combined earth's magnetic field and the magnetic field created by a current carrying conductor wire.

### 1.3 Magnetic Field - Terminology

As discussed later, the boundary conditions and the magnetization of a magnetic shield are such that the magnitude and direction of the resulting magnetic field within the shield may be significantly different than the magnitude and direction of the magnetic field which generated the resulting field. In this study, the resulting field within the shield will be referred to as the applied magnetic field, and the magnetic field which generated the resulting field will be referred to as the triggering field.

For the purpose of this thesis, two triggering fields are defined; the earth's magnetic field, referred to as the external triggering field (etf), and the magnetic field created by the current flow in the conductor, referred to as the internal triggering field (itf). Both the internal and external fields will create an applied field. Using the superposition principle (Lorrain and Corson, 1970:43), it is possible to treat each applied field independently, and the net or actual magnetic field within the shield will be the vector sum of the two applied fields.

### 1.4 Report Outline

This study is limited to static magnetic field. In the SCEP potential applications the magnetic shield will be submitted to the earth's magnetic field and the magnetic field created by a

continuous current carrying conductor. These fields are static, however, the spacecraft's relative motion with respect to the earth's magnetic field modifies the problem from strictly static fields to non-static fields. The effect of the relative motion of the spacecraft with respect to the earth's field is not discussed in this thesis, nonetheless, the effect is expected to be mainly back emf.

Chapter 2 qualitatively discusses the possibility of shielding a magnetic force. Typically, a magnetic shield is a ferromagnetic material with a very high permeability. Accordingly, to demonstrate a magnetic shield's ability to reduce the induction of the magnetic force upon itself and the shielded conductor, it is necessary to review the properties of ferromagnetic and high permeability materials when submitted to a triggering field.

Chapter 3 quantitatively determines the magnitude of the magnetic force induced on the shield and the shielded conductor. It defines a shield geometry which is best suited for the SCEP, and discusses its limitations. Performance criteria are developed to evaluate the SCEP potential for space applications. Accordingly, a comparison of the SCEP and an electric thruster is also included in this Chapter. Finally, when the current level is varied to achieve a desired thrust profile, it is likely that a residual magnetic field will accumulate within the shield, thereby degrading its performance. This issue and a method to manage the residual field are also discussed.

Chapter four describes an experiment designed to verify the theoretical findings of Chapter two. The aim of this experiment is to demonstrate the feasibility of shielding a magnetic force.

Chapter five contains a summary of the findings of this feasibility study and recommendations for further investigation.

## II. Shielding a Magnetic Force

### 2.1 Ferromagnetism

2.1.1 Introduction. Ferromagnetic materials are characterized by their strong permanent magnetic moments, even in the absence of a triggering field (Johnk, 1975:151). In 1907, Weiss postulated and later confirmed experimentally that a ferromagnetic material in an overall unmagnetized state consists of many small, essentially totally magnetized domains. Each domain is randomly oriented so that the sum of all magnetic fields is approximately equal to 0. Domain sizes have been found to range from a few microns to a millimeter across. Weiss further postulated that strong intrinsic coupling or interaction forces exist between adjacent atoms to provide the fully magnetized state within a given domain. In 1928, Heisenberg of Germany and Frenkel of the USSR independently verified, using quantum theory, that the extraordinarily strong forces holding the domain atoms in parallel alignment is attributable to the coupling forces between the net electron spins of the adjacent atoms (Heisenberg, W. 1928:49). The walls between the domains are transition regions for the spin alignments of the adjacent domains, and they are of the order of 100 atoms thick (Johnk, C.T.A. 1975: 151). As the strength of a triggering magnetic field applied to a ferromagnetic material is increased, the domain walls move to favor the growth of those domains having magnetic moments aligned with the applied field (Figure 4). This movement of walls is reversible by decreasing the field if the amplitude of

the triggering field is not too large. For a sufficiently large triggering field, the domain magnetic moments rotate until essentially all moments are oriented parallel with the applied field. This condition is called saturation. This paragraph has described qualitatively the nature of a ferromagnetic material with and without a triggering magnetic field present. The following paragraphs offer a more quantitative description of this behavior.

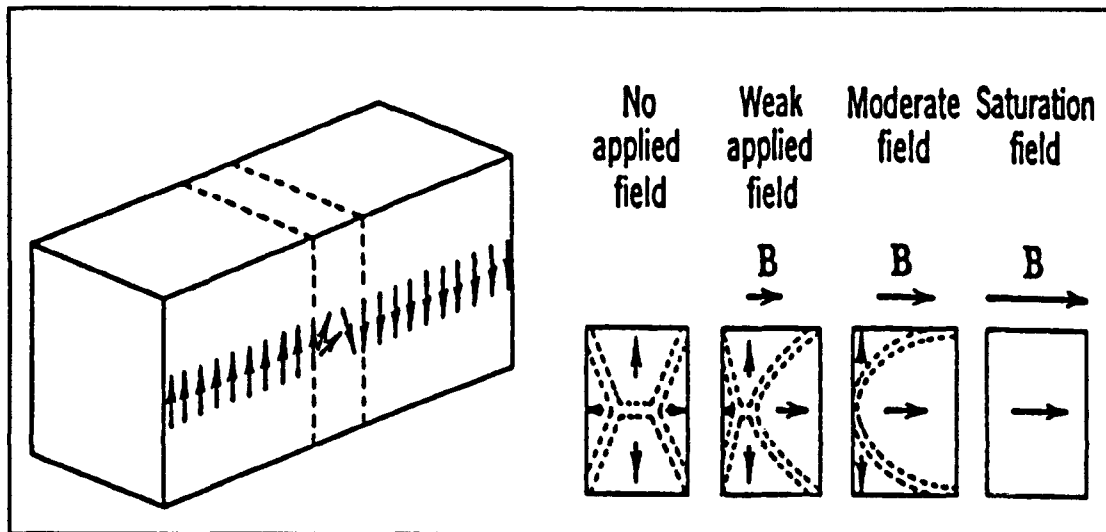


**Figure 4.** Electron's spin submitted to external triggering field (Johnk, 1975:152).

2.1.2 Magnetic Field Intensity ( $H$ ) vs Magnetic Field Density ( $B$ ). The relation between the magnetic field intensity and the magnetic field density in an isotropic medium is given by (Krauss J.D. 1984:169):

$$H_a = \frac{B_a}{\mu} \quad (3)$$



where  $\mu$  is the permeability of the medium, and the subscript "a" indicates that the equation is valid as long as B and H are in the same medium. For ferromagnetic materials, as we will see, the permeability and hence the relative permeability varies with the intensity of the applied magnetic field.

2.1.3 Magnetization. As suggested earlier, in the presence of a triggering field, the electron spin axis within a ferromagnetic material will tend to align in the direction of the applied field. The ordered alignment of those spin axis' will result in the apparent creation of a second magnetic field within the shield. This field is referred to as the magnetization field  $\underline{M}$ . Figure 5 illustrates a ferromagnetic material magnetized by a triggering field. For an isotropic medium, the magnetization is obtained using the following relation (Herbert and Neff 1981:231):

$$\underline{M} = (\mu_r - 1) \underline{H}_{app} \quad (4)$$

where

$\underline{M}$  = magnetization vector (amp/m);

$\underline{H}_{app}$  = the applied magnetic field vector (amp/m);

$\mu_r$  = relative permeability of the material; and

the relative permeability is given by (Krauss J.D. 1984:215):

$$\mu_r = \frac{\mu}{\mu_0} \quad (5)$$

where

$\mu_r$  = relative permeability of the medium; and

$\mu_0$  = permeability of vacuum.

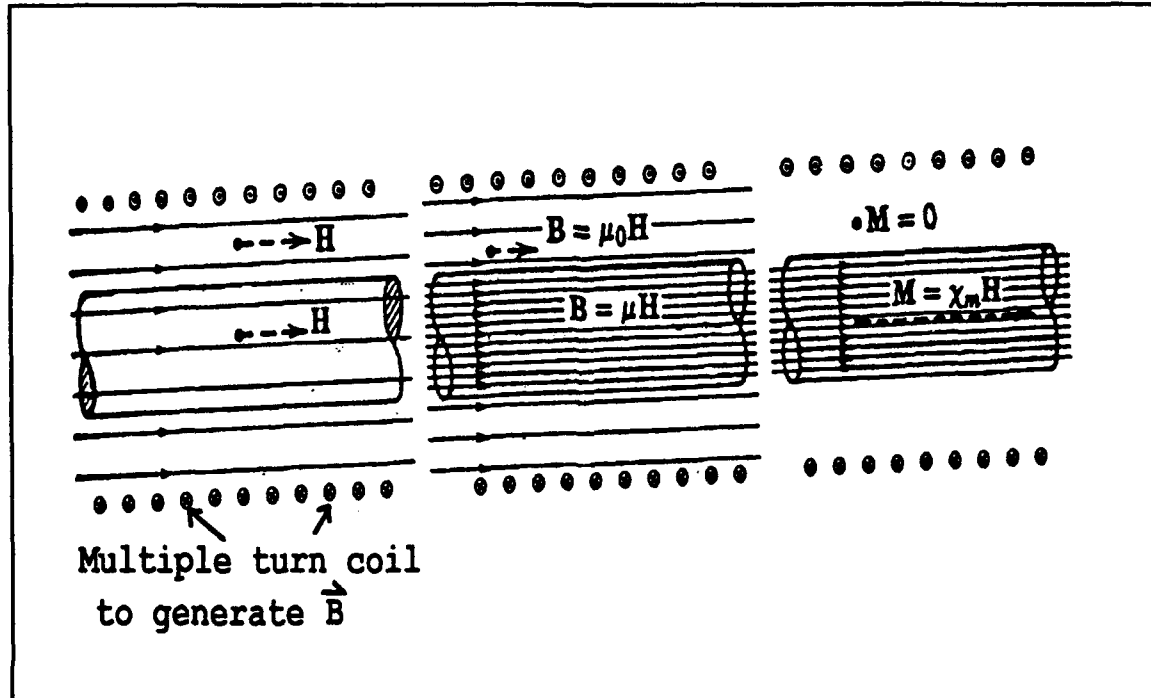


Figure 5. Magnetization field within magnetized iron rod (Johnk, 1975:1522).

Also, for the purpose of modelling the magnetization field as a surface magnetic current density, it is possible to approximate the magnetic moment of each spin by an equivalent small current loop. As can be seen in the cylindrical section of magnetized material in Figure 6, neighboring current densities created by the magnetic moment cancels out except for an apparent surface current referred to as the magnetic surface current density ( $J_{sm}$ ). The surface magnetic current density is given by (Johnk, C.T.A. 1975:146):

$$\underline{J}_{sm} = \underline{n} \times \underline{M} = \chi_m \underline{n} \times \underline{H}_{app} \quad (6)$$

where

$\chi_m$  = the magnetic susceptibility of the material;

$\underline{J}_{sm}$  = the surface magnetic current density (amp/m); and

$\underline{n}$  = the unit vector normal to the surface.

$$\chi_m = (\mu_r - 1) \quad (7)$$

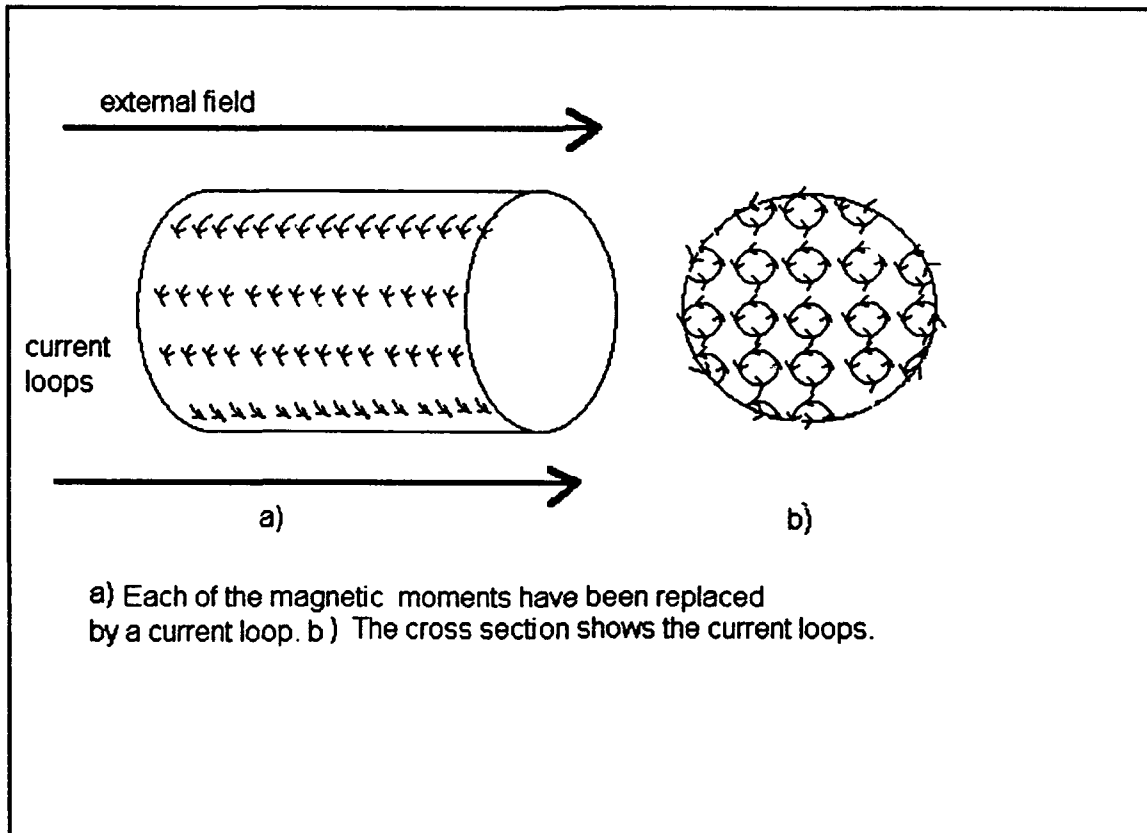


**Figure 6.** Surface magnetic current density.

The modelling of the magnetization field by a magnetic surface current density will prove useful later as we determine the effect of the magnetization field on the magnetic shield's performance.

2.1.4 B&H Curve - Relative Permeability  $\mu_r$ . As discussed earlier, the triggering field will result in an applied field, and the presence of the applied field will create a magnetization field. Accordingly, the applied magnetic field density ( $B_{app}$ ) will be proportional both to the applied and to the magnetization field, and it is given by (Herbert and Neff 1981:231):

$$B_{app} = \mu_0 (H_{app} + M) \quad (8)$$

Using equation (3) and equation (5) it is possible to express the applied magnetic field density ( $B_{app}$ ) in terms of the relative permeability and of the applied magnetic field ( $H_{app}$ ), as given by:

$$B_{app} = \mu_0 \mu_r H_{app} = \mu H_{app} \quad (9)$$

The relation between  $B_{app}$  and  $H_{app}$  is non-linear and it is given by a magnetization curve, also known as the B&H curve. The slope of this curve is defined as the incremental permeability (Johnk, C.T.A. 1975:154). A typical magnetization curve for a ferromagnetic material submitted to a triggering field for the first time is illustrated at Figure 7. This curve is referred to as the initial magnetization curve. The magnetization curve is modified when the triggering field is re-applied after having been removed. This change is due to the lagging of the applied magnetic field density

behind the magnetizing force, and is known as the hysteresis effect. Therefore, the relative permeability of a ferromagnetic material is not constant but a function of both the applied magnetic field, and the previous magnetic history of the material (Figure 8).

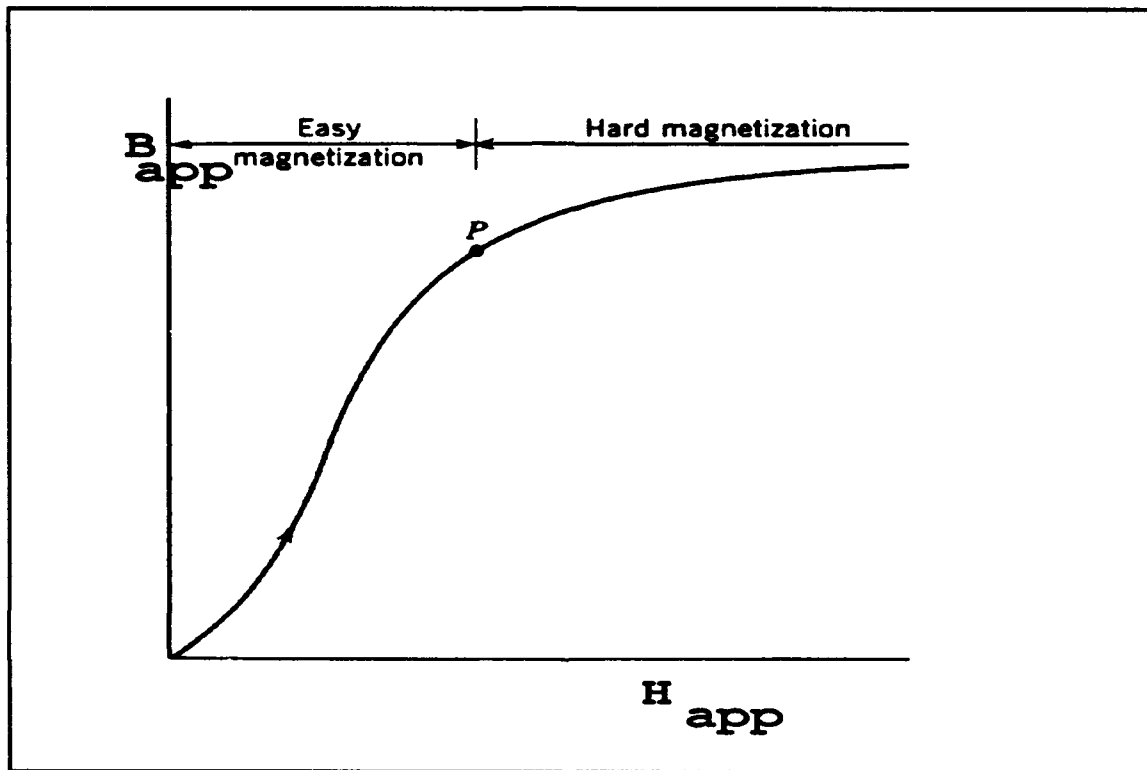


Figure 7. Initial magnetization curve. (Krauss J. D., 1984:242)

2.1.5 Initial Magnetization. The initial magnetization curve may be divided into two regions; the "easy magnetization" region, and the "hard magnetization" region. Recall that the nature of the interaction between the walls of the material and the applied magnetic field is to re-orient the magnetic moment of the electron spins in the same direction as the applied field, thereby resulting in a magnetization field. Therefore, the magnetization of the material is proportional to the number of walls. The easy

magnetization region is characterized by a steep slope which is due to the fact that a large number of walls are available to interact with the applied magnetic field. Accordingly, magnetization of the material is achieved relatively easily and the applied magnetic field density ( $B_{app}$ ) increases significantly as the applied magnetic field ( $H_{app}$ ) increases. The hard magnetization region is characterized by the shallower slope of the magnetization curve which suggests that the number of walls has decreased significantly. Therefore, further magnetization of the material becomes more difficult. That is the rate at which  $B_{app}$  increases for a given increase in  $H_{app}$  is significantly less than the rate at which  $B_{app}$  increases in the easy magnetization region.

2.1.6 B&H - Hysteresis. Now we will focus our attention on the behavior of the applied magnetic field density ( $B_{app}$ ) when the

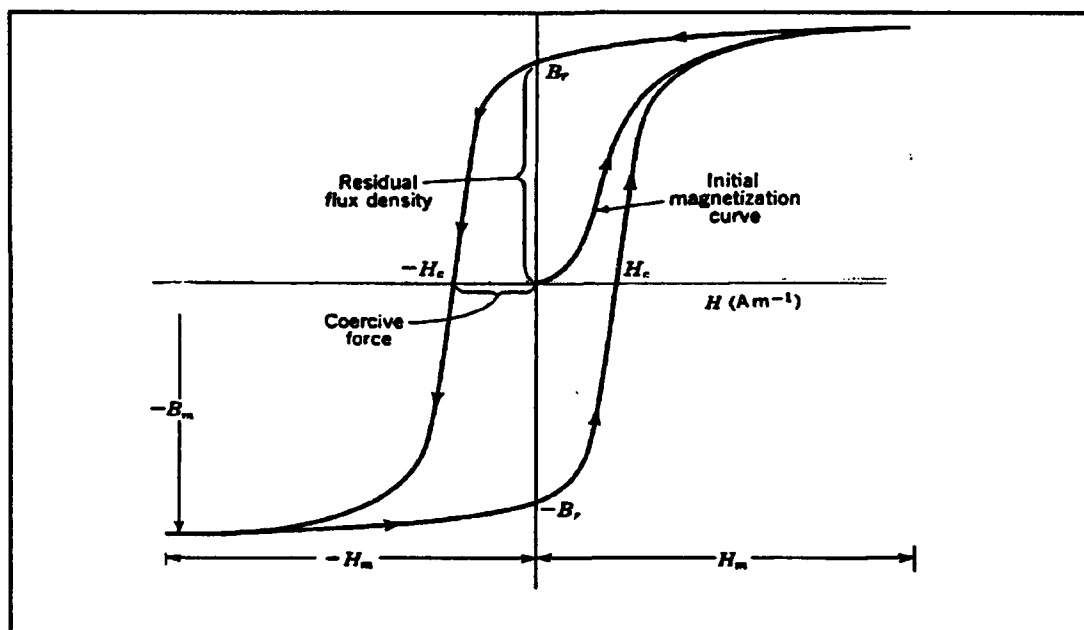


Figure 8. Hysteresis effect. (Krauss J. D., 1984:246)

applied magnetic field ( $H_{app}$ ) is removed from the material. As indicated earlier, due to the hysteresis effect  $B_{app}$  lags behind  $H_{app}$ . Figure 8 illustrates this behavior.

First, consider a demagnetized ferromagnetic material, i.e.  $B_{app}=0$ . When a small  $H_{app}$  is applied and then removed we note that the  $B_{app}$  returns to zero. Therefore no hysteresis effect is observed. This region is referred to as the "reversible wall motion" region (Figure 9). When the  $H_{app}$  is increased beyond the reversible wall motion region and then removed, we observe that a permanent magnetic field density ( $B_{r1}$ ) is retained within the material. Also, in this region the incremental permeability increases. This region is defined as the "irreversible wall motion" region. Finally, when  $H_{app}$  is increased even further and then removed we note that an even higher permanent magnetic field density ( $B_{r2}$ ) is retained within the material. This region is defined by a decrease in the incremental permeability and is referred to as the "irreversible magnetization rotation" region. Incremental permeability reaches a constant value when the material is magnetically saturated. Any magnetic field density ( $B_r$ ) retained within the material is referred to as the residual magnetic field density. If the polarity of the applied magnetic field is reversed, we note that a magnetic field of intensity  $H_c$  will reduce  $B_r$  to zero.  $H_c$  is referred to as the "coercive force".

Equations (3) through (9) are valid for an isotropic medium, that is, the magnetization field is assumed to be in the same direction as the applied magnetic field. This assumption is correct for the initial magnetization curve. However, when  $H_{app}$  is removed

and re-applied in the opposite direction  $\underline{B}_{app}$  will maintain its original direction until  $\underline{H}_{app} = -\underline{H}_c$ . Accordingly, in this region  $\underline{H}_{app}$  and  $\underline{B}_{app}$  are no longer in the same direction, and the medium is no longer considered isotropic.

In this study, we assume that the material is isotropic; this assumption is based on the following arguments. In the design of the SCEP a shaking coil is considered; the purpose of this coil is to demagnetized the shield. The presence of the coil tends to significantly decrease the magnitude of  $\underline{H}_c$  to a point where the hysteresis effect becomes negligible (Baum and Bork, 1991:73). Accordingly,  $\underline{H}_{app}$  will almost continually have the same direction as  $\underline{B}_{app}$  and the material will behave as an isotropic material.

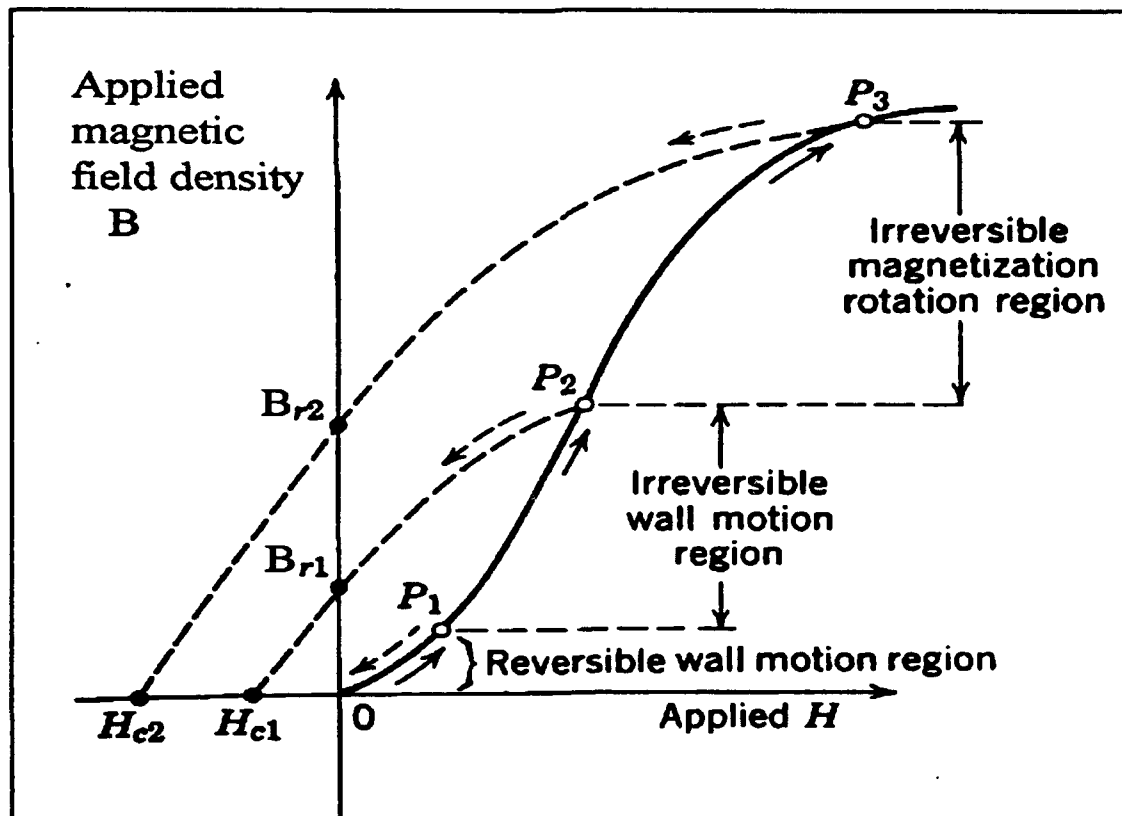


Figure 9. Wall motion regions. (Johnk C.T.A., 1975:153)



## 2.2 High Permeability Material

2.2.1 Boundary Effect. Now we investigate the behavior of a magnetic field at the boundary between a low and a high permeability medium. In a single medium the magnetic field is continuous. However, at the boundary between two media of different permeabilities, the magnetic field may change abruptly both in magnitude and direction. The following relation describes the change in direction (Krauss, J. D. 1984: 236):

$$\frac{\tan \alpha_1}{\tan \alpha_2} = \frac{\mu_1}{\mu_2} = \frac{\mu_{r1}}{\mu_{r2}} \quad (18)$$

where

$\mu_1$  = the permeability of medium 1;

$\mu_{r1}$  = the relative permeability of medium 1;

$\mu_2$  = the permeability of medium 2;

$\mu_{r2}$  = the relative permeability of medium 2;

$\alpha_1$  = the angle of incidence, measured normal to the boundary, at which the field travel in medium 1; and

$\alpha_2$  = the transmitted angle, measured from the normal to the boundary at which the field travel in medium 2

2.2.2 Vacuum/Shield Boundary. Consider the case of a magnetic field with its source in the vacuum (medium 1), where the relative permeability is 1, and a magnetic shield (medium 2), where the relative permeability may vary from 8,000 to 450,000. For these conditions, the ratio of the relative permeability will be extremely small, which suggests that for almost any angle of incidence the transmitted angle will be close to 90 degrees. For example, let:

$$\mu_{r1} = 1 \quad (\text{vacuum})$$

$$\mu_{r2} = 30,000 \quad (\text{relative permeability of a magnetic shield}),$$

then the value of the transmitted angle for different angles of incidence may be computed using equation(10), and tabulated (Table II). As expected, the transmitted angle will be greater than 89.9 degrees for any incident angle greater than 10 degrees.

**Table II.** Incident vs transmitted angle with  $\mu_r = 30,000$ .

$\alpha_1$ (degree)	$\alpha_2$ (degree)	$\alpha_1$ (degree)	$\alpha_2$ (degree)
9.000	89.998	0.00090	25.232
10.000	89.989	0.00100	27.636
11.250	89.990	0.00113	30.500
12.857	89.992	0.00129	33.948
15.000	89.993	0.00150	38.146
18.000	89.994	0.00180	43.384
22.500	89.995	0.00225	49.675
30.000	89.997	0.00300	57.518
45.000	89.998	0.00450	67.003
90.000	90.000	0.00900	78.819

Conversely, consider the source of a magnetic field to be in the high permeability medium, the shield (medium 1), into a vacuum (medium 2). In this case, the ratio of the relative permeability will be very high, which suggests that for almost any angle of incidence the transmitted angle will be normal to the boundary. Figure 10 illustrates the influence of these boundary conditions on the field orientation and magnitude for a medium of relative permeability 9 times greater than the other medium. In this

**THIS  
PAGE  
IS  
MISSING  
IN  
ORIGINAL  
DOCUMENT**

## 2.3 Magnetic Field Around Magnetic Shield

2.3.1 Introduction. Based on the preceding discussion, it is possible to describe the magnetic field behavior in and around a cylindrical shield. As stated earlier, the magnetic shield will be exposed to both the external triggering field and the internal triggering field. We will address this problem by independently studying the case of a magnetic shield exposed to an external magnetic field and the case of a shield exposed to an internal field. Then, using the superposition principle (Lorrain, P. and Corson, R.C. 1970: 43), we will combine the effects of both magnetic fields to obtain the total magnetic field within and around the shield. Throughout this section we will assume that the shield is adequately demagnetized. In chapter 3 we will discuss a technique which may be employed to ensure that the coil is indeed demagnetized.

2.3.2 Magnetic Shield - External triggering Field. First, recall that at the boundary between the vacuum and the shield, most of the applied magnetic field will tend to remain parallel to the surface of the shield after penetration, and a small portion of the external triggering magnetic field will penetrate the shield and maintain a direction normal to the shield. The applied field will tend to orient the electron spin axis to be parallel to the shield surface, thereby creating a magnetization field which in turn may be modelled as a magnetic surface current density. This current will create a magnetic field inside and outside of the shield. Accordingly, the net magnetic field outside the shield will be equal

to the sum of the external triggering field and the magnetic field created by the magnetic surface current density.

Now consider a cylindrical shield with its axis perpendicular to the external triggering magnetic field. Based on the previous discussion, it may be viewed that most of the external field will penetrate the outer surface of the shield following a direction essentially parallel to the surface of the shield and exiting to free space and turning to produce a uniform distribution. Simultaneously, the electron spin axis will be re-oriented and create a magnetization field within the shield, and a magnetic surface current density which in turn will create a magnetic field inside and outside the shield's surface. This is conceptually illustrated at (Figure 10).

Accordingly, the magnetic field inside the cylindrical shield will be the sum of the field created by the surface magnetic current density and that portion of the external triggering field which, due to its very small angle of incidence, will successfully leak through the shield into the shielded region. This is illustrated in Figure 10, where the one flux line with an angle of incidence of zero is seen to penetrate the inner surface of the shield. Only a very small part of the external triggering field will reach the conductor wire. Accordingly, the induced magnetic force that would have been exerted on the conductor wire in the absence of the shield will be greatly reduced by the shield's presence. The magnitude of the field inside the shield will be determined analytically in Chapter 3. Figure 12 is an accurate representation of the magnetic field in and around a magnetic shield

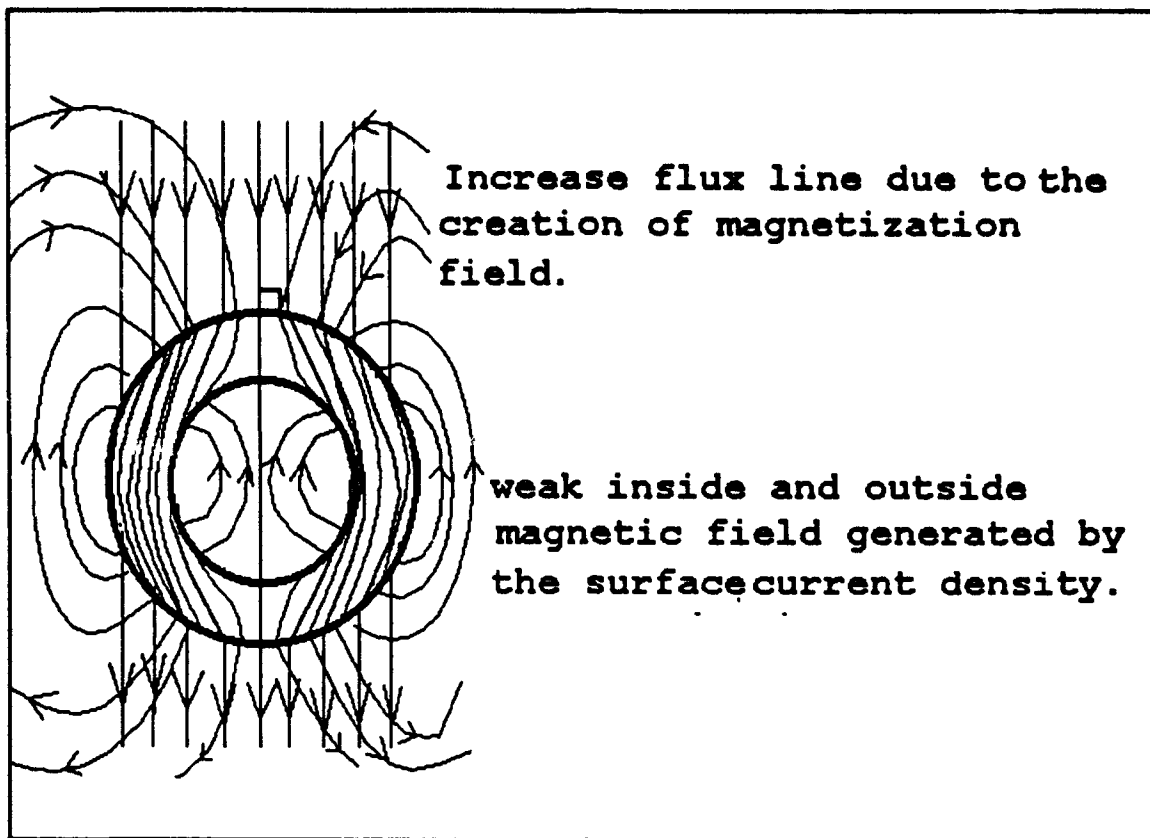


**Figure 11.** Conceptual illustration of the external and induced fields in and around a cylindrical shield.

of relative permeability equal to 50.

We will now focus our attention on the nature of the interaction between the external triggering magnetic field and the magnetic shield in order to demonstrate that no force or torque will be exerted on the shield itself.

As discussed previously the effect of the applied field on the magnetic shield is to redirect the orientation of the electron spin axis. Each electron spin may be modelled as a current loop (Krauss, J. D. 1984: 215). Accordingly, a magnetic shield exposed to a magnetic field is similar to current loops exposed to a magnetic field. In such a case, electromagnetic theory indicates

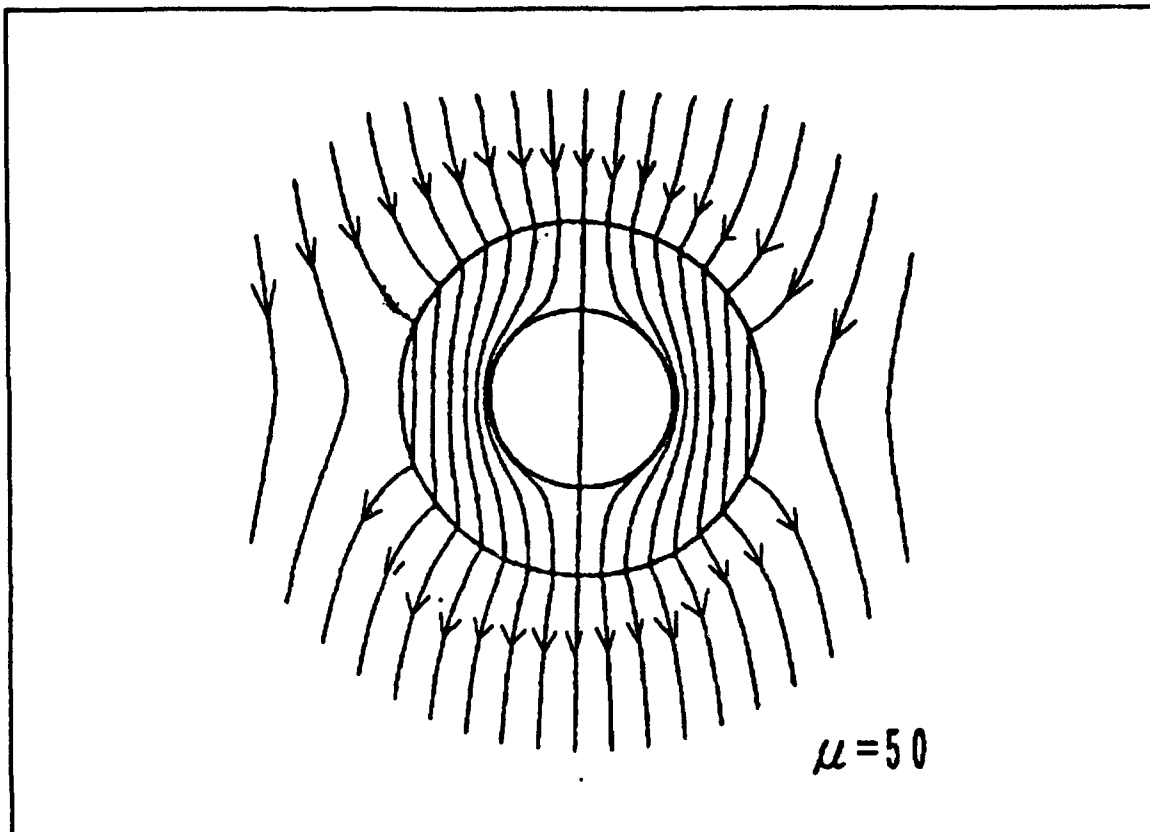


**Figure 12.** Equation derived field in and around a cylindrical shield for  $\mu_r = 50$ . (Rikitake T., 1990:1232)

that the loop will experience a torque, and this is given by (Lorrain and Corson, 1970:365):

$$\tau = I B S \sin\theta \quad (11)$$

where

$\tau$  = the torque experienced by the current loop (N/m);

$S$  = the area enclosed within the current loop ( $\text{m}^2$ );

$I$  = the current circulating in the loop (amp);

$B$  = the magnetic field (tesla); and

$\theta$  = the angle between the magnetic moment of the loop and the direction of the magnetic field (rads).

Note that the vector notation has been dropped. As we will see shortly, it is not necessary to apply equation (11) to complete the demonstration.

Accordingly, when an electron's spin axis is already aligned with the applied field, and hence  $\theta = 0$ , no torque is experienced. However, when an electron's spin is not aligned with the applied field, the electron's spin will experience a torque which will tend to align the spin in the direction of the applied field. As discussed in the first section of this chapter, in a demagnetized shield the spins are randomly oriented from one domain to another, therefore, the sum of all torques will be near zero.

Accordingly, the only kinetic interaction between the external triggering field and the magnetic shield will result in the application of torque on electron spin axis, and given the random orientation of the spins no net torque will be experienced. No net force will be induced on the shield due to the external triggering magnetic field.

2.3.3 Magnetic Shield - Internal Triggering Field. An infinitely long and straight current carrying conductor wire will produce a circular magnetic field in a plane normal to the axis of the wire. The direction of the field is obtained using the right hand rule, and the magnitude field is given by (Herbert and Neff, 1981: 190):

$$H_{wf}(\rho) = \frac{I}{2 \pi \rho} \quad (12)$$

where



$I$  = the current circulating in the wire (amp); and  
 $\rho$  = the distance from the conductor axis (m).

This equation may be used as an approximation for a conductor of finite length as long as the overall length of the conductor is much greater than the distance  $\rho$ .

When a cylindrical shield is placed around the conductor, the internal magnetic field will remain unchanged until it reaches the shield. This result is explained at Appendix A. Inside the shield, the magnetic field will behave in a manner similar to the one described in the case of the external triggering field. The field near the surface of the shield will penetrate the shield and will tend to remain parallel to the shield surface. This applied internal triggering field will in turn create a magnetization field which may be modelled as magnetic surface current density. This surface current density will also generate a magnetic field.

2.3.4 Combining the fields. Two magnetic fields will be present within the shield. Using the principle of superposition, the net applied field will be equal to the vector sum of the two applied fields. Since both applied fields are approximately parallel to the surface of the shield, the vector sum is reduced to the sum of the magnitude of each applied field on one side of the shield, and the difference in magnitude of the two fields on the other side of the shield (Figure 13). The combined applied magnetic field may be treated as a single field. As discussed previously, the interaction between an applied magnetic field and a shield is characterized by the re-orientation of randomly oriented electron

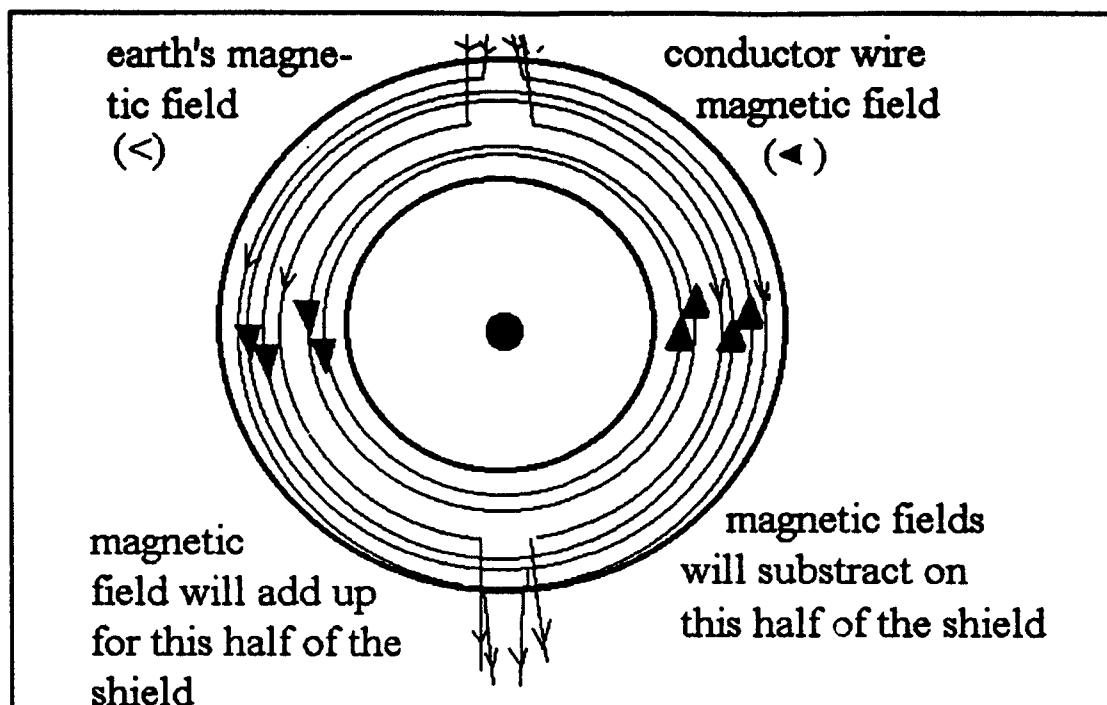


**Figure 13.** Conceptual illustration of the combined fields within a cylindrical shield.

spin moment. Each re-orientation is equivalent to a torque, and due to the random orientation of the spin moments, the sum of all torque will be approximately zero. Accordingly, it may be concluded that no force will be induced on the shield due to the combined effect of the external and internal magnetic triggering fields on the electron spin moments within the shield. However, secondary fields and surface current densities will be created, and these have the potential to interact with the current carrying conductor or the external triggering field and create a net force. The magnitude of these interactions will be determined in Chapter 3.

#### 2.4 Summary

In this Chapter we reviewed the magnetic properties of a high permeability ferromagnetic material. This review was limited to

the case of a demagnetized shield exposed to a uniform homogeneous external triggering field and an internal triggering field created by a current carrying conductor wire. This review indicated that the transition from a low permeability medium such as vacuum to a high permeability medium such as a magnetic shield allows for a redirection of the magnetic field. It is this ability to redirect the field which creates an region of greatly reduced magnetic field, that is the shielded region. Also, the review indicated that the interaction between the shield and the triggering magnetic fields is such that the applied field will induce a torque on randomly oriented domains of electrons spin axis within the shield. Therefore, no significant force or torque is expected upon the shield. This is a significant result and deserves further comments.

The ability to shield the magnetic force is due to the nature of the interaction from which the force results. Consider the gravitational interaction between two bodies; it is characterized by the magnitude of their mass and the vector joining the two bodies. Accordingly the gravitational force exerted on each body is equal and opposite in direction. We note that the instantaneous gravitational force acting on each mass is independent of their relative velocity. In the case of magnetic interaction it is significantly different. The magnetic force induced on a moving particle by another moving particle is a function of the net charge of each particle, the distance between the particles, and their velocities. Therefore, the force exerted on a moving charge is characterized by the motion of the charge. Accordingly, in the case of the shielded conductor, the force that acts on a current carrying

conductor wire is diffused by a force acting on a charge in circular motion, that is the electron's spin axis, therefore resulting in a torque rather than in a net force.

Finally, this review was conducted on a qualitative basis and under the assumption that no residual field existed within the shield. In Chapter 3 we discuss shielding on a more quantitative basis by defining shield efficiency factor. A technique to manage the residual magnetic field will also be discussed.

### III. Shielding Effectiveness

#### 3.1 Introduction

In Chapter 2 we established that no significant force will result from the interaction of an applied magnetic field and the electron spin moments within a magnetic shield. However, secondary fields and surface current densities will be created. Three potential interaction sources are identified:

1. the portion of the external triggering which successfully leaks through the shield into the shielded region. This field is referred to as the "residual external triggering field ( $H_{retf}$ )". The  $H_{retf}$  will induce a force on the current carrying conductor;
2. the magnetic surface current density ( $J_{sm-etf}$ ) created by the external triggering field will generate a magnetic field inside and outside the shield. The inside magnetic field will also induce a force on the current carrying conductor; and
3. the external triggering field will induce a force on the magnetic surface current density ( $J_{sm-itf}$ ) created by the internal triggering field.

Therefore, the purpose of this chapter is to determine the magnitude of those interactions.

3.1.1 Shielding Factor. Magnetic shielding may be defined as the process of preventing a magnetic field from entering or leaving an region protected by a magnetic shield. As seen in

Chapter 2 perfect shielding cannot be achieved. A measure of the magnetic shield efficiency is defined as the shielding efficiency S:

$$S = \frac{H_{\text{unshielded } A}}{H_{\text{shielded } A}} \quad (13)$$

where

$H_{\text{unshielded } A}$  = the magnetic field within region A when this region is unshielded;

$H_{\text{shielded } A}$  = the magnetic field within region A when this region is shielded; and

the subscript "A" indicates that the magnetic field is measured over the same region.

3.1.2 Cylindrical Geometry. A cylindrical shield offers the best geometry for the problem of shielding a conductor wire. This geometry is well suited to envelope a conductor while using the minimum amount of shield. It also allows us to introduce simplifying assumptions in the application of Laplace's and Poisson's equations. These simplifications yield the development of a closed form analytical expression for the magnetic field around and within the magnetic shield. Without those simplifications, the magnetic field would have been evaluated using numerical analysis approximation, thereby rendering the problem analysis more complex. Figure 14 illustrates the cylindrical shield and the associated nomenclature.

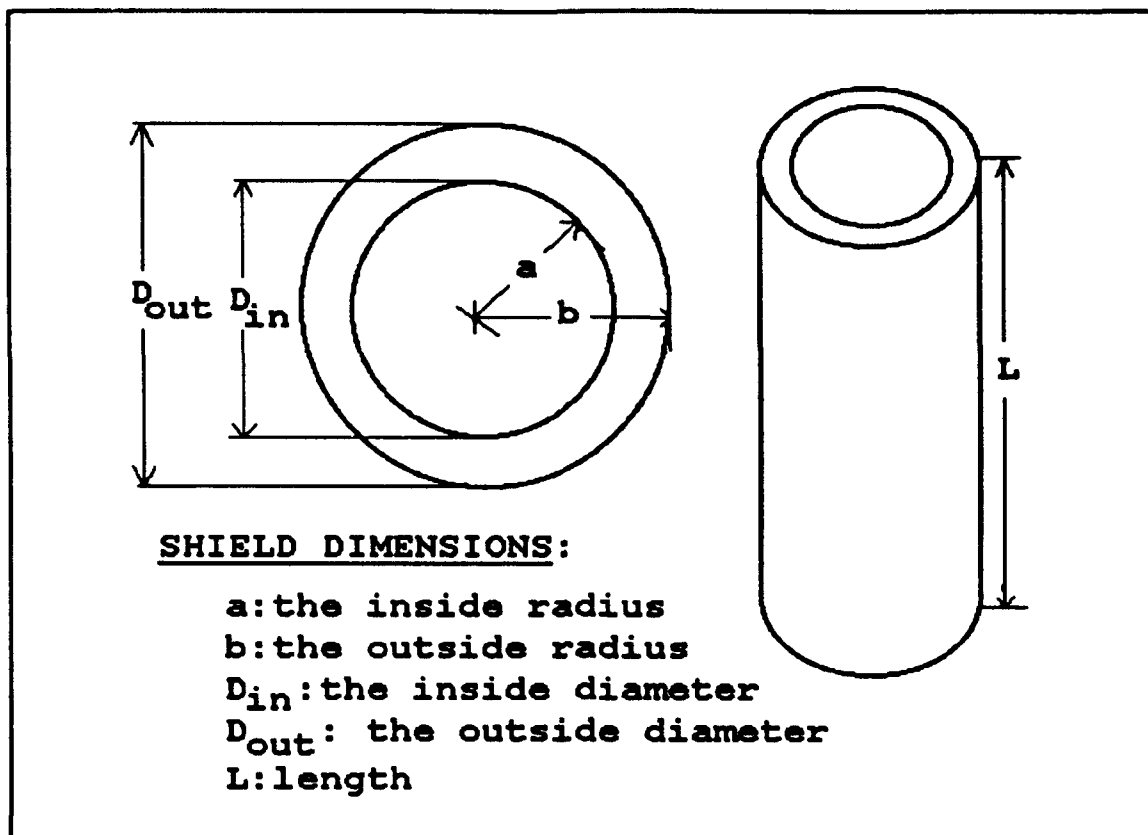
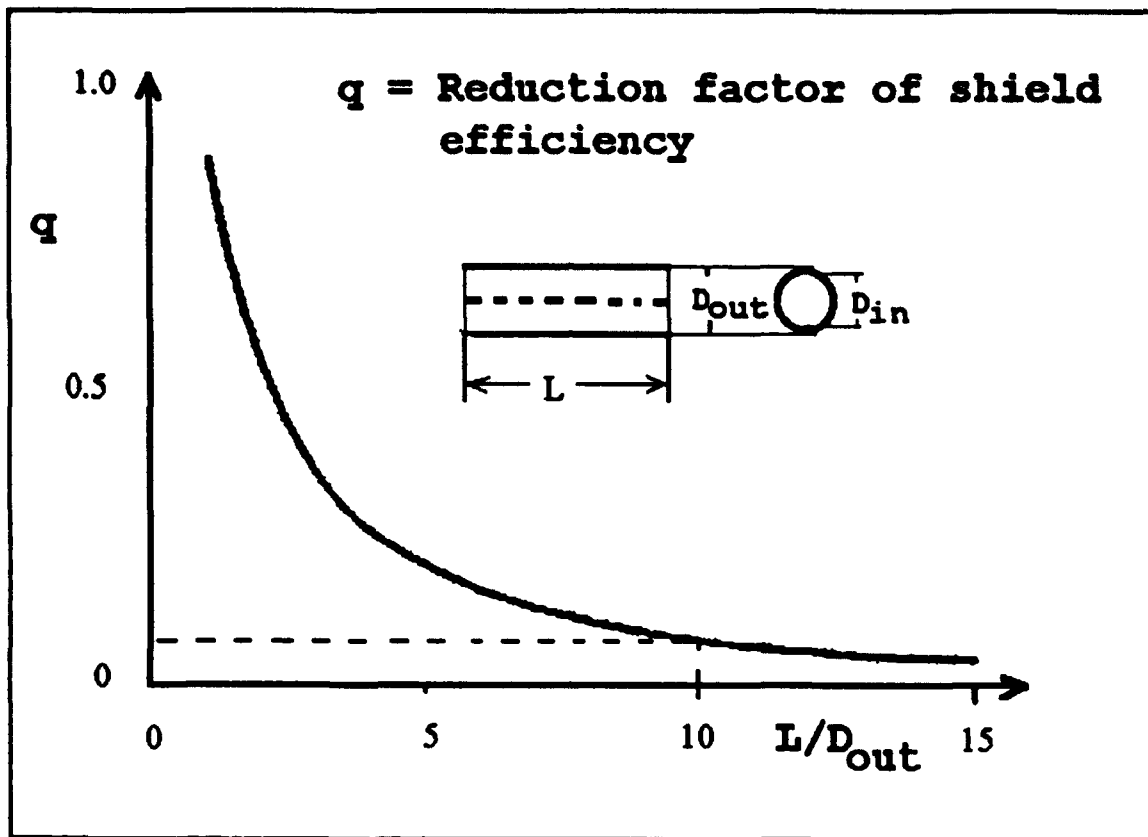


Figure 14. Cylindrical shield nomenclature.

**3.1.3 End Effects.** Mager discusses the issue of end effects for a cylindrical shield (Mager, J.A., 1970). The end effects reduce the overall shielding efficiency; however, as the ratio of the length of the cylindrical shield over its diameter increases, the end effects become negligible. Figure 15 is a graphical representation of the shielding factor efficiency reduction (ordinate) as a function of the overall length to diameter ratio. The reduction in efficiency is less than 0.1 when a ratio of 10 or greater is achieved. End effects may also be decreased by sealing the end of the cylinder with caps built from the shield material.



**Figure 15.** Cylindrical shield efficiency vs length/diameter (Mager, 1970:68).

3.1.4 Applied Magnetic Field - Vector Notation. As indicated before, due to the boundary conditions, the applied magnetic field in a high permeability material will be aligned nearly parallel to the shield's surface. Accordingly, the applied magnetic field direction may be determined by the angle at which the triggering fields penetrate the shield. Therefore, the vector notation will be dropped for the discussion of the applied magnetic field, with the assumption that it may readily be determined when required.



### 3.2 Residual External Triggering Field

3.2.1 Introduction. The  $H_{\text{ref}}$  may be determined using equation (13) and the  $H_{\text{ext}}$ , it is given by:

$$H_{\text{ref}} = \frac{H_{\text{ext}}}{S} \quad (14)$$

Accordingly, to determine the magnitude of the force generated by  $H_{\text{ref}}$  it is necessary to determine the shield efficiency  $S$ .

As discussed previously, two magnetic fields are present and act upon the magnetic shield. It is evident that the aim of the shield is to prevent the external field from entering the shielded region. Consequently, we are not concerned with the magnetic shield's ability to prevent the internal magnetic field from leaving the shielded region. However, as discussed in Chapter 2 the presence of internal triggering field will modify the applied magnetic field density, which, as discussed later, is proportional to the shield efficiency. In order to determine the shield efficiency of a cylindrical shield exposed to an external and internal field, we will first determine the shield efficiency for the limited case of a cylindrical shield exposed to an external triggering field. We will then determine the effect of the internal field on the applied magnetic field density, and the shield efficiency.

### 3.2.2 Shield Efficiency - External triggering Field.

Albrecht J. Mager discussed the problem of a cylindrical magnetic shield exposed to a uniform homogeneous external triggering magnetic field (Mager, J.A. 1970:67). Neglecting the end effect associated with the cylindrical geometry, and assuming that the relative permeability of the shield is much greater than the relative permeability of the medium surrounding the shield, the shielding factor for the shielded region is given by

(Mager, J.A. 1970:68):

$$S = \frac{1}{4} \mu_r \left( 1 - \frac{D_{in}^2}{D_{out}^2} \right) + 1 \quad (15)$$

where

$D_{in}$  = the inside diameter of the cylindrical shield;

$D_{out}$  = the outside diameter of the cylindrical shield; and  
in the case of a magnetic shield;

$$\frac{1}{4} \mu_r \left( 1 - \frac{D_{in}^2}{D_{out}^2} \right) \gg 1 \quad (16)$$

accordingly equation (15) may be rewritten as:

$$S = \frac{1}{4} \mu_r \left( 1 - \frac{D_{in}^2}{D_{out}^2} \right) \quad (17)$$

Typically, the relative permeability of the shield runs between 5,000 to 450,000, and the relative permeability of the vacuum is 1. Therefore, the assumption stated above is generally satisfied.

The relative permeability of the shield is a function of the applied magnetic field, more precisely, as given by equation (3). Therefore, the shielding factor may be written in terms of  $H_{app}$ ,  $B_{app}$  and the dimensions of the shield:

$$S = \frac{1}{4} \frac{B_{app}}{\mu_0 H_{app}} \left( 1 - \frac{D_{in}^2}{D_{out}^2} \right) \quad (18)$$

Accordingly, to determine the shielding factor it is necessary to know the applied magnetic field and the applied magnetic field density. Recall that for a ferromagnetic material the relation between  $B_{app}$  and  $H_{app}$  may be obtained using the B&H curve of the shielding material. Accordingly, only  $B_{app}$  or  $H_{app}$  is needed to compute the shielding factor if the B&H curve of the shield is known.

3.2.3 Applied Magnetic Field Density - External triggering Field. In the case of a cylindrical shield immersed in a uniform and homogeneous magnetic field ( $H_{ext}$ ) the applied magnetic field density is given by (Magnetic Shield Corporation Catalog Lk-2g, 1991:2):

$$B_{app-ef} = \frac{\mu_0 1.25 D_{out} H_{ef}}{t} \quad (19)$$

where

$B_{app-ext}$  = the applied magnetic field density due to the external triggering field;

$\mu_0$  = the permeability of vacuum =  $1.26 \times 10^{-6}$  (henry/m)

$H_{ext}$  = the external triggering magnetic field; and

$t$  = the thickness of the shield in units common to  $D$ .

Using the B&H curve of the shield, it is possible to determine the applied magnetic field and compute the shield efficiency for the simple case of a cylindrical shield immersed in a uniform and homogeneous external triggering magnetic field.

3.2.4 Applied Magnetic Field Density - Internal Field. In the case of an infinitely long cylindrical shield exposed to an internal field such as the one created by a current carrying conductor, the applied magnetic field density is given by<sup>1</sup>:

$$B_{app-ief} = \frac{\mu_0 H_{ief} (D_{out}^2 + D_{in}^2)}{(D_{out}^2 - D_{in}^2)} \quad (20)$$

where

$B_{app-int}$  = the magnetic field density within the shield due to the internal triggering field (tesla);

---

<sup>1</sup>This expression is derived using Laplace's equation. The development is provided at Appendix A.

$H_{itr}$  = the internal triggering magnetic field (amp/m).

3.2.5 Applied Magnetic Field Density - Total. As discussed in Chapter 2, the applied magnetic field density at any point will be approximately the vector sum of the two applied fields. Because both applied fields density will be approximately parallel to the circumference of the shield surface, the vector sum of the two fields density will either be a sum or a difference of the magnitudes of each applied field densities. Accordingly, one half of the magnetic shield will experience a field density  $B_1$  approximately equal to:

$$B_1 \approx B_{app-ist} + B_{app-est} \quad (21)$$

and the other half of the shield will experience a field density  $B_2$  approximately equal to:

$$B_2 \approx B_{app-ist} - B_{app-est} \quad (22)$$

As illustrated in Figure 13, the field to the left of center is labelled  $B_1$ ; and the field to the right is labelled  $B_2$ . For the SCEP application it should be noted that the difference between  $B_1$  and  $B_2$  will be small, since the earth's magnetic field will be smaller than the magnetic field created by a current carrying conductor wire.

Therefore, the presence of an internal magnetic field will modify the magnetic field density, and consequently the shield efficiency. Typically, the magnetic shield dimensions and efficiency is computed using the worst case scenario, which is based on the highest magnetic field density anywhere in the shield. This will ensure that the shield is not saturated at any point. Saturation of the shield indicates that electron spin axis of all domain are oriented in the direction of the applied field. Therefore, if the applied field is further increased the shield relative permeability decreases. Consequently, the shield efficiency will also decrease.

Accordingly, using equations (14), (18) and (21) the  $H_{ref}$  may be expressed as:

$$H_{ref} = \frac{H_{ef}}{\frac{1}{4} \mu_r \left( 1 - \frac{D_{in}^2}{D_{out}^2} \right)} \quad (23)$$

where  $\mu_r = B_1 / H_1$ , recall equation (21) defines  $B_1$ . From this equation and the assumption that a shield relative permeability is much greater than one, it may be conclude that  $H_{ref} \ll H_{ef}$ . An example will illustrate this conclusion.

3.2.6. An Example. Consider the coil described in section

1.1.1, that is:

1. 1 (m) X 0.25 (m) rectangular coil;
2. 0.05 (cm) diameter of the conductor wire;

3. 1000 turns = diameter of the coil = 2 (cm); and
4. 1 (amp) current circulates in the conductor.

A cylindrical shield is then placed over one of the two 1 (m) segments of the rectangular loop. The dimensions of the shield are:

1.  $L = 1$  (m) the length;
2.  $D_{in} = 3$  (cm) the inside diameter; and
3.  $D_{out} = 3.06$  (cm) the outside diameter.

$H_{ref}$  is obtained using equation (23). The inside and outside diameter are defined, the earth's magnetic field at LEO is the external magnetic field. For the purpose of this example, the earth's magnetic field is considered uniform and homogeneous, accordingly:

$$H_{ref} = 24.6 \text{ (amp/m)}$$

The relative permeability remains to be determined. As discussed in Chapter 2, the relative permeability of a shield is a function of the applied magnetic field density, and it is obtained using the magnetization curve of the material. For this example, the shield is "co-netic" material for which the magnetization curve is known (Magnetic Shield Corporation Catalog Lk-2g, 1991:2). As defined previously, the applied magnetic field density is  $B_1$ . Using equation (19), (20) and (21)  $B_1$  may be expressed as:

$$B_1 \approx \frac{\mu_o H_{ref} (D_{out}^2 + D_{in}^2)}{(D_{out}^2 - D_{in}^2)} + \frac{\mu_o 1.25 D_{out} H_{ref}}{t} \quad (24)$$

where

$$t = (D_{out} - D_{in}) / 2 = 0.03 \text{ (cm)}; \text{ and}$$

$$H_{itr}(D_{in}/2) = n I / \pi D_{in} = 10,610 \text{ (amp/m)}^2$$

Therefore,

$$B_1 = 0.675 \text{ (tesla)} + 0.004 \text{ (tesla)} = 0.679 \text{ (tesla)}$$

Using the magnetization curve for "co-netic" material yields:

$$\mu_r = 100,000$$

Accordingly,

$$H_{ref} = \frac{H_{eff}}{971} = 0.025 \text{ (amp/m)}$$

Therefore, for this particular example, the force induced on the conductor wire due to the residual external field will be approximately 1,000 times smaller than the force acting on an unshielded conductor.

### 3.3 Magnetic Surface Current Density - $H_{etr}$

3.3.1 Estimating  $J_{sm-etr}$ . The magnetic surface current density created by  $B_{app-etr}$  is not uniform. This is due to the fact that  $B_{app-etr}$  is not uniform. As illustrated in Figure 12  $B_{app-etr}$  has approximately the same direction on both sides of the shield. Accordingly, the direction of the surface current on the outer surface of the shield will be opposite from one side to the other.

---

<sup>2</sup>The internal triggering field will vary only slightly between the inner and outer surface of the shield. Therefore, it is assumed to be constant throughout the shield. The value of this approximation is discussed at Appendix A.



This suggests the presence of two transition regions where the current density will vary from its peak value in one direction to zero, and back to its peak value but this time in the opposite direction. Numerical analysis methods are required in order to describe the current density behavior accurately. However, we are interested in an estimate of the current density's magnitude. Therefore, we assume that the transition regions are infinitely small. Accordingly, the magnitude of the current density created by  $B_{app-ef}$  is considered uniform and equal to the peak value. Also, this assumption allows the magnetic surface current density to be modelled as two independent current densities with equal but opposite direction. Using this assumption, the magnitude of the current density may be determined by solving Laplace's equation<sup>3</sup>.

$$J_{s \ m-ef} = \frac{4 D_{out}^2 H_{ef}}{(\mu_r (D_{out}^2 - D_{in}^2) + (D_{out}^2 + D_{in}^2))} \quad (26)$$

Accordingly, the magnetic surface current density created by the external field is also inversely proportional to the permeability of the shield. This surface current density may be modelled as an equivalent current. The magnitude of this current is given by:

$$I_{sm-ef} = J_{sm-ef} \pi D_{in} \quad (27)$$

---

<sup>3</sup>The development of Laplace's equation is similar to the development illustrated at Appendix A.

The magnitude of the magnetic field created by this equivalent current at the current carrying conductor position is given by equation (12):

$$H_{sm-ef} \left( \frac{D_{in}}{2} \right) = \frac{J_{sm-ef} \pi D_{in}}{\pi D_{in}} = J_{sm-ef} \quad (28)$$

And the magnitude of the force induced on the conductor wire due to the density current created by the external field is given by Lorentz equation (2):

$$F_{sm-ef} = I B_{sm-ef} L = I \mu_o J_{sm-ef} L \quad (29)$$

Therefore, the force generated on the conductor wire due to the magnetic surface current density generated by the external field will be significantly less than the force exerted on an unshielded current carrying conductor.

3.3.2 An Example. Consider the scenario developed in the previous example (section 3.2.6). The same value are used to compute the magnetic surface current density:

$$J_{sm-ef} = \frac{H_{ef}}{971} = 0.025 \text{ (amp/m)} \quad (30)$$

Accordingly, for this example the current density will be approximately 1,000 times smaller than the external triggering field. And, the magnitude of the force is:

$$F_{sm-ef} = 3 \times 10^{-5}(N) \quad (31)$$

Therefore, the force induced on the conductor wire as a result of the equivalent current is also approximately 1,000 times less than the force induced on an unshielded conductor.

### 3.4 Magnetic Surface Current Density - $H_{if}$

3.4.1 Estimating Current. The magnitude of the magnetic surface current density resulting from an internal field is given by<sup>4</sup>:

$$J_{sm-if} = \frac{H_{if} (D_{out}^2 + D_{in}^2)}{\mu_r (D_{out}^2 - D_{in}^2)} \quad (32)$$

This surface current density may be modelled as an equivalent current. The magnitude of this current is given by:

$$I_{sm-if} = J_{sm-if} \pi D_{out} \quad (33)$$

This current will be significantly smaller than the current being shielded since it is inversely proportional to the relative permeability of the shield. And the magnitude of the force induced on the shield due to this equivalent current is given by Lorentz equation (2):

---

<sup>4</sup>This result is obtained using Laplace's equation. This development is included at Appendix A.

$$F_{sm-ig} = I_{sm-ig} B_{ef} L \quad (34)$$

Therefore, this force is also significantly less than the force exerted on the current carrying conductor.

3.4.2 An Example. Again using the value of the previous example it is possible to calculate the current which models the surface current density.

$$I_{sm-ig} = \frac{I_{cond}}{1941} = 0.515 \text{ (amp)}$$

Accordingly, for this example, the equivalent current induced on the shield will be approximately 2,000 times smaller than the current circulating in the conductor. And the magnitude of the force is:

$$F_{sm-ig} = 1.6 \times 10^{-5} (N) \quad (36)$$

Therefore, the force induced on the shield as a result of the equivalent current is also approximately 2,000 times less than the force induced on an unshielded conductor.

### 3.5 SCEP Performance

In this section we will calculate a number of the characteristics associated with the SCEP. These characteristics will serve as a comparison basis to evaluate the potential performance of the SCEP. The performance evaluation of the SCEP is difficult to obtain using standard criteria such as specific

impulse. Indeed, the SCEP does not expel mass to obtain thrust, therefore, theoretically the specific impulse would be infinity. Accordingly, specific impulse is not considered an appropriate criteria for comparison. Perhaps a more significant criteria is the maximum thrust obtainable per unit mass of the propulsion system. For the purpose of this thesis, the propulsion system does not include the power system. The power required to achieve maximum thrust is also considered as a performance criteria.

Finally, the SCEP performance criteria will be compared to an electric propulsion thruster currently being developed. It must be emphasized that the performance criteria are calculated for a rudimentary design of the SCEP, that is the design is not optimized. Also, as indicated in Chapter 1 the magnetic field are considered to be static for this feasibility study. Therefore, the force calculated in the performance criteria does not take into consideration the effect of the back emf experience by the SCEP when moving relative to the earth's magnetic field. Therefore, the purpose of the comparison is to illustrate the SCEP performance potential for space applications.

3.5.1 An Application. In order to calculate the performance criteria we will use the examples considered thus far. Let's review the parameter of this example:

1. rectangular coil;
2. 1000 turns;
3. conductor diameter - 0.05 (cm);
4. dimensions - 1 (m) X 0.25 (m);
5. current - 1 (amps);

6. shield inside diameter - 3 (cm); and

7. shield outside diameter - 3.06 (cm).

In this application 3 of the 4 segments forming the rectangular coil will be shielded, leaving one segment of 1 (m) exposed to the earth's magnetic field. The following information is required to complete the calculation of the performance criteria:

1.  $\rho_{shield} = 8.74$  (gm/cm<sup>3</sup>), the density of the shielded material;

2.  $\rho_{alu} = 2.70$  (gm/cm<sup>3</sup>), the density of aluminum; and

3.  $r_{alu} = 2.8 \times 10^{-8}$  (ohm m), the resistivity of aluminum.

The mass of the SCEP is the sum of the shield mass and the wire mass, and the power requirement is the power dissipated due to the conductor wire resistivity. The mass of the shield is given by:

$$\begin{aligned} m_{shield} &= Volume_{shield} \rho_{shield} \\ &= 1.5(m) \times 0.3(mm) \times 2\pi \times 1.515(cm) \times 8.74(g/cm^3) \\ &= 0.376 (kg) \end{aligned} \tag{37}$$

Similarly, the mass of the conductor wire is given by:

$$\begin{aligned} m_{wire} &= Volume_{condu} \rho_{alu} \\ &= 1000 \times 2.5(m) \times \pi (0.025(cm))^2 \times 2.7(g/cm^3) \\ &= 1.33 (kg) \end{aligned} \tag{38}$$

And the power requirement will be given by:

$$\begin{aligned}
 P_{SCEP} &= I^2 R = I^2 r_{alu} \frac{Length_{condu}}{Surface_{condu}} \\
 &= (1(amp))^2 \times 2.8 \times 10^{-8} (ohm \ m) \times \frac{2500(m)}{\pi (0.025(cm))^2} \\
 &= 0.357 \ (Kwatt)
 \end{aligned} \tag{39}$$

Finally, the maximum thrust is given by:

$$F_{max} = B_{ef} I L_{expos} n = 0.03 \ (N) \tag{48}$$

where

$n$  = the number turn in the coil; and

$L_{expos}$  = the length of the conductor wire exposed to the earth's magnetic field.

Table III provides a crude comparison of the performance criteria for both the SCEP and an electric thruster. The SCEP offers other obvious advantages, such as simplicity of design which would make the SCEP extremely reliable. Therefore, it may be concluded that the SCEP has a significant potential to outperform current propulsion systems.

### 3.6 Shield Shaking

3.6.1 Shield's Magnetization. Magnetization of the shield will occur as a result of the hysteresis phenomena observed within

**Table III. SCEP Performance Potential.**

---

<u>SCEP</u>	<u>Electric Thruster*</u> (Janson, 1993:2)
$F_{max} = 0.03 \text{ (N)}$	$F_{max} = 0.020 \text{ (N)}$
$m = 1.8 \text{ (kg)}$	$m = 21 \text{ (kg)**}$
$\text{Power} = 0.357 \text{ (KW)}$	$\text{Power} = 0.7 \text{ (KW)}$

\* The specifications are for an electric thruster currently being developed.

\*\* The mass of 21 kg does not include the mass of propellant and propellant tank.

---

the shield. First, consider a demagnetized shield to which a magnetic field is applied ( $H_{app}$ ). The magnetic field density within the shield will be as given by the B&H curve of the material. When  $H_{app}$  is removed a residual magnetic field density (Figure 8) is retained within the shield.

As discussed before, a magnetic field within the shield will result in a surface magnetic current density. After the applied magnetic field is removed, a surface current will remain on the surface of the shield. Therefore, when the magnetic field is re-applied, it will interact with the surface current and a magnetic force would be induced on the shield. While the surface current created by the residual field is significantly smaller than the current circulating in the conductor wire, it will nonetheless be sufficient to induce a significant force on the shield. This was



observed during the laboratory experiment. Also, to achieve maximum shield efficiency, the shield should be operated close to saturation. Accordingly, it is expected that the residual field will approximate its maximum value, thereby degrading the performance of the magnetic shield. Techniques such as shaking coil (O. Väinö, R. Peltonen, and Börje Rantala, 1980: 575-578) have been developed to prevent the magnetization of a shield.

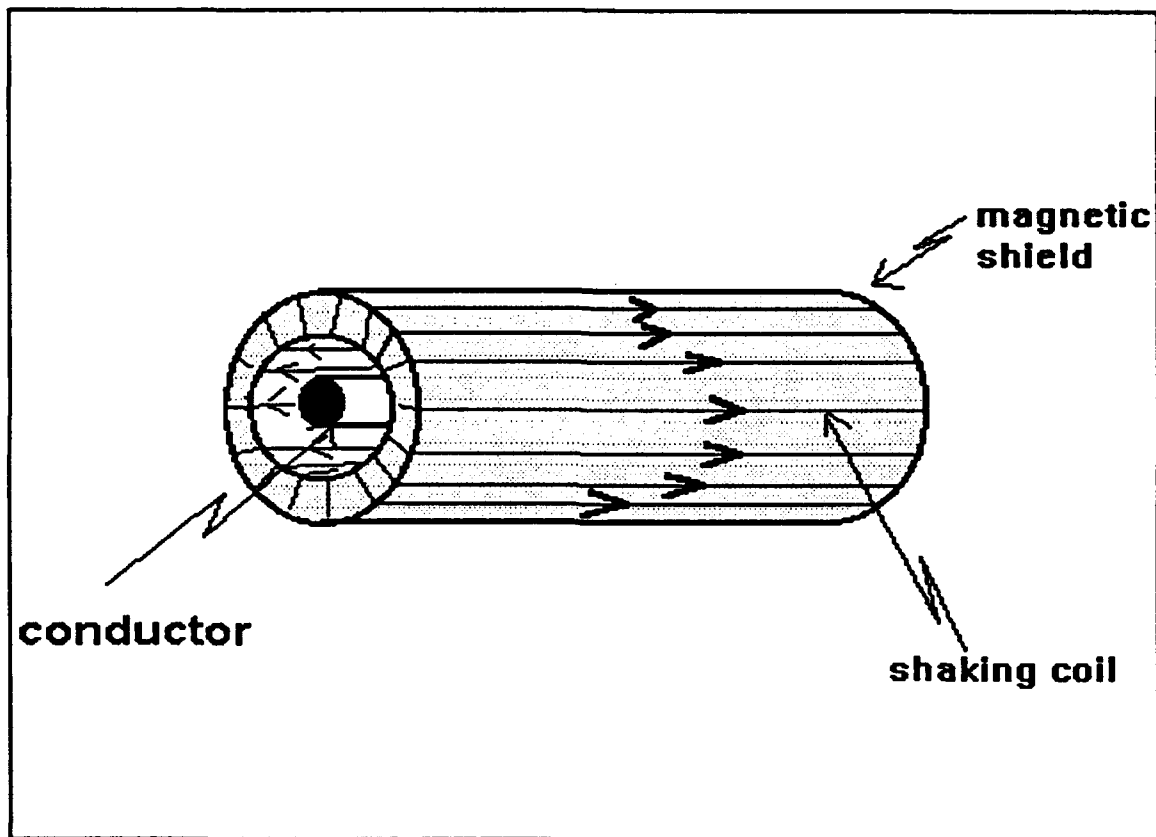


**Figure 16.** Shaking coil wrapped around a cylindrical shield.

3.6.2 Shaking Coil. The purpose of a shaking coil is to reduce the hysteresis effect within a magnetic shield. It is a coil loosely wrapped to conduct current along the inner and outer surfaces of the shield so as to induce a circumference magnetic field within the shield. Use of alternating current causes the

induce field to alternate in direction (Figure 16). It has been demonstrated that the shaking coil parameters such as the frequency and the current intensity are not critical to its efficiency (Kelhä, Peltonen, and Rantala, 1980:578). To illustrate the working principle of a shaking coil, consider a shield that has been magnetized. When a low amplitude magnetic field is applied and removed a number of times, we observe that the hysteresis effect can be used to our advantage by reducing the residual field to zero. Figure 17 is an approximate illustration of shield demagnetization process. The shaking coil will produce the required low intensity magnetic field which will vary in polarity with the frequency of the current. For every cycle, the residual magnetic field density will decrease. The amount by which residual magnetic field decreases ( $\Delta B_i$ ) is proportional to the magnitude of the residual field. Therefore,  $\Delta B_i$  will decrease as the residual field decreases. When the residual field reaches a value close to zero, it will retain this value until a magnetic field is re-applied. Typically, a shaking coil uses a frequency of 50 hz and current of 0.75 amps.

### 3.7 Summary

In this chapter we reviewed the equations required to determine the magnitude of the forces induced on a shielded conductor and concluded that those forces are negligible. Also, performance criteria were defined in order to estimate the SCEP potential for space applications. These criteria were used to compare the SCEP with an electric thruster. It was found that the SCEP compared most favorably to the electric thruster. Finally, we discussed a technique called shaking coil that may be employed in

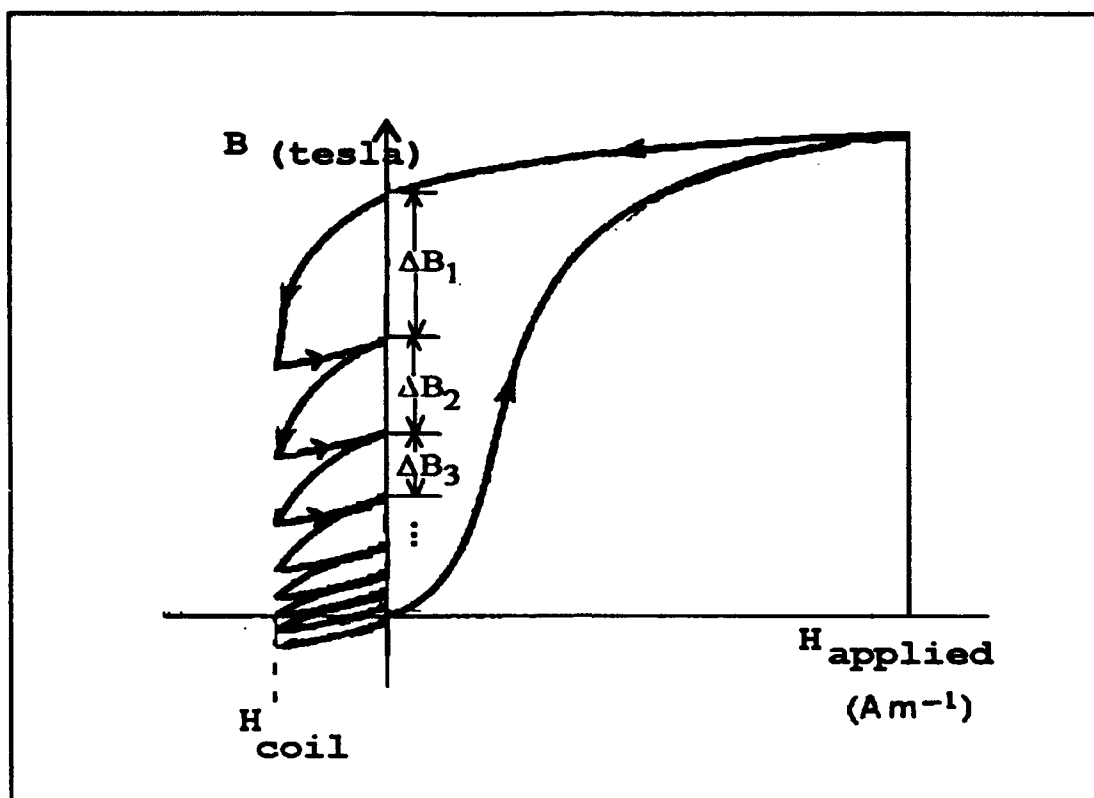


**Figure 17.** Demagnetization process.

order to maintain the shield's performance.

## IV. Experimental Demonstration

### 4.1 Introduction

4.1.1 Aim. The aim of the experimental demonstration is to provide visual evidence to support this feasibility study. In particular, it demonstrates that a magnetic shield may be used successfully to prevent a magnetic field from inducing a magnetic force upon a current carrying conductor wire and its shield. Accordingly, the purpose of the experiment is to visually observe a displacement, due to induced magnetic force, in the absence of a magnetic shield, and, to observe a significant reduction in the magnitude of this displacement when the shield is present.

4.1.2 The Space Environment. The experimental demonstration should reflect, as much as possible, the environment in which the shield will be exposed, specifically the relative field strengths. For electrodynamic propulsion in Low Earth Orbit (LEO) the shield will be exposed to a relatively weak external triggering magnetic field, the earth's magnetic field, and a relatively intense internal magnetic field, the field created by current carrying conductor wire. We will define this characteristic as the magnetic field ratio. While this ratio will vary significantly as the demand in current changes, it may still be estimated to be approximately 300<sup>5</sup>.

---

<sup>5</sup>This ratio corresponds to a current in a conductor wire of 1000 amps and a shield radius of 2.35 cm. The internal magnetic field will then be 90 Oersted while the earth's magnetic field is approximately 0.3 Oersted.

## 4.2 Design Considerations

4.2.1 Induced Magnetic Force. The most basic experiment necessary to observe the induced magnetic force would probably consist of a current carrying conductor wire segment exposed to a magnetic field. For this type of experiment the induced magnetic force is given by equation (2):

$$F = (I \times B) L \quad (2)$$

Using this equation it may be shown that a single current carrying conductor wire exposed to a magnetic field is not a practical experiment to conduct. For example, consider a magnetic field of an intensity comparable to the earth's magnetic field, and a 10 cm long conductor wire. A current of approximately 33,000 amps is required in order to produce 0.5 Newton. Even if the magnetic field is increased by a factor of 100, it would still be necessary to produce a current of 330 amps to obtain 0.5 Newton. Also, with this design it would be difficult to visually observe a displacement of the wire. Accordingly, an alternative design is proposed. This design allows for a significantly large current to circulate while maintaining the ability to visually observe the effect of a small force.

4.2.2 Coil and Torque. The torque experienced by a current carrying conductor loop exposed to a constant magnetic field is given by equation (11):

$$\tau = I B S n \sin\theta$$

(11)

Accordingly, it may be preferable to conduct the experiment using a multiple-turn loop, since the torque can be increased by increasing the number of turns in the loop. For example, a single wire carrying 1000 (amps) current may be replaced by a wire carrying a 1 amp current in a coil made of 1000 turns.

4.2.3 Torque vs Force. The feasibility of a SCEP is based on the ability to reduce the induced magnetic force on the shielded segments of a loop. The proposed experiment suggests that torque reduction will be measured rather than the induced magnetic force. While this is apparently a correct statement, this experimental design will still allow us to achieve the aim of the experiment; that is to visually demonstrate that a magnetic force may be significantly reduced by a magnetic shield. Indeed, the torque experienced by the loop is the sum of the induced magnetic forces acting on different segment of the loop. Accordingly, if no torque is experienced by the loop when the segments are independently shielded, then it may be concluded that the induced magnetic force has been shielded.

4.2.4 Generating a Magnetic Field. Two Helmholtz coils were built and used to generate a constant magnetic field over a sufficiently large region. The intensity of the magnetic field is approximated by (Fink, Donald G. and Carroll, 1968):

$$H = \frac{0.8992 N I}{R} \quad (41)$$

where

H = the magnetic field (Oersteds);

N = the number of turns per coil;

I = current (amps); and

R = is the radius of the coil (cm).

This approximation is valid as long as the distance between the two coil is less than the radius of the coil. In the experiment this was satisfied since the radius of the Helmholtz coils was 15.5 (cm) and the distance between the two Helmholtz coils was 13.3 (cm).

The direction of the magnetic field will depend on the direction of the current circulating in the Helmholtz coil. This direction may be obtained using the right hand rule, where, as illustrated in Figure 18, the magnetic field is estimated to be mostly parallel to the cylinder axis. The actual distribution of the magnetic field is not precisely known. This is not considered a significant factor, since the aim of the experiment is to demonstrate the possibility of significantly reducing the induced magnetic force. Accordingly, whether the induced magnetic force results from a uniform or a non-uniform field is not pertinent to this laboratory demonstration. However, it is important that the magnetic field remains constant for the duration of the experiment. This allows us to assume that the center coil is exposed to the same magnetic field when shielded and unshielded. The magnetic field generated by the Helmholtz was kept constant by maintaining the

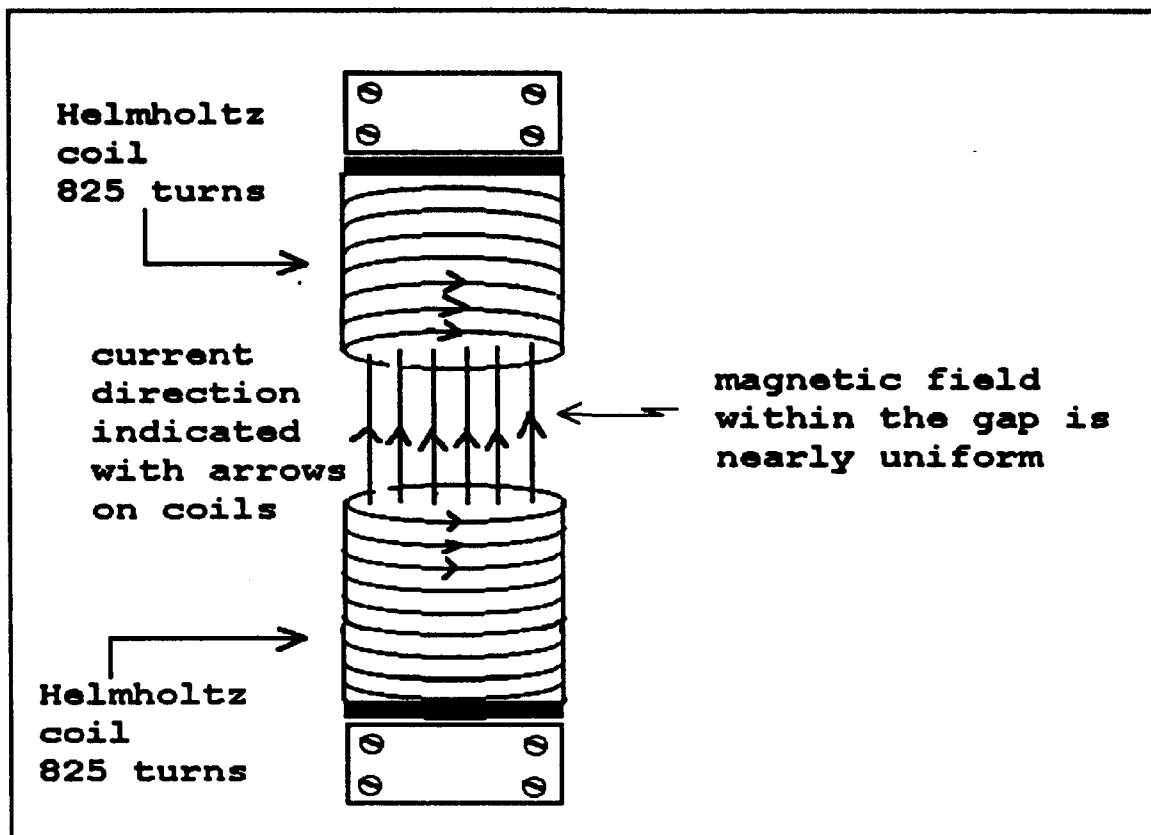


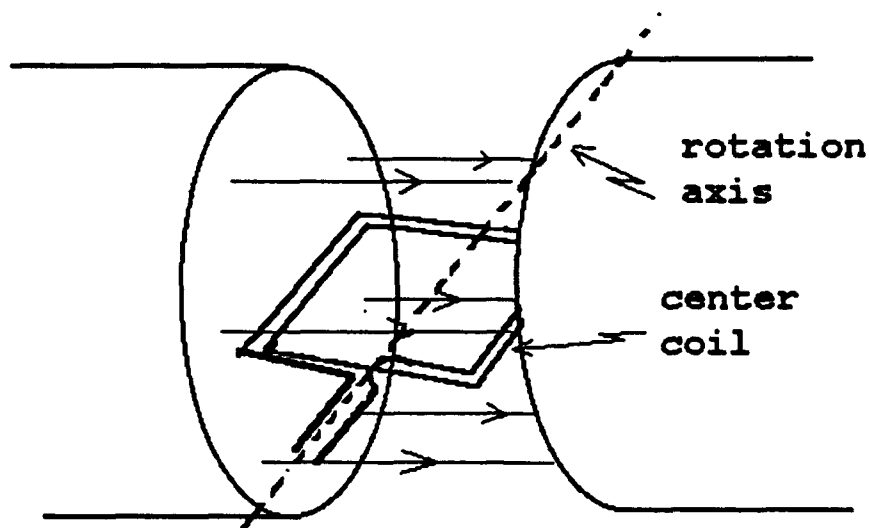
Figure 18. Field generation by a pair of Helmholtz coils.

current and the distance between the two coils constant.

4.2.5 Measurements. The method of measurement is to record the magnitude of the center coil rotation about its axis when subjected to the magnetic field created by the Helmholtz coils ( $H_{ext}$ ). The torque induced on the center coil is proportional to  $\sin \theta$ , where  $\theta$  is the angle formed by the direction of the  $H_{ext}$  and the vector normal to the plane defined by the center coil segments. This plane is referred to as the "coil plane". Therefore, a maximum torque is exerted on the center coil when the coil plane is parallel to  $H_{ext}$  (Figure 19). In the absence of friction the torque decreases as a function of  $\sin \theta$ , and equals zero when the coil plane reaches a position normal to the magnetic field.



Multiple-turn loop exposed to magnetic field generated by two Helmholtz coils.



Maximum torque is exerted when the center coil is parallel to the magnetic field.

Figure 19. Center coil placement in the magnetic field.

During the manipulation we observed that bearing friction would equal the torque for an unshielded center coil, when  $\theta$  reached a value of approximately  $135^\circ$  to  $150^\circ$ . Accordingly, a relative measure of the torque exerted on the center coil for different scenario (i.e. when the coil is unshielded versus shielded) may be obtained by assuming that the friction in the bearing will remain constant for the duration of the experiment. This is accomplished by first considering the expression which describes the equilibrium between the electrodynamic torque and the friction torque,  $\tau_F$ :

$$B_{eff} i n S \sin(\theta_F) = \tau_F \quad (42)$$

THIS  
PAGE  
IS  
MISSING  
IN  
ORIGINAL  
DOCUMENT

If the friction torque remains constant, a ratio of the induced magnetic force for a shielded coil over an unshielded center coil is given by:

$$SFR = \frac{F_{ef-unshielded}}{F_{ef-shielded}} = \frac{\sin\theta_{F-shield}}{\sin\theta_{F-unshielded}} \quad (45)$$

This ratio will be referred to as the shielded force ratio (SFR).

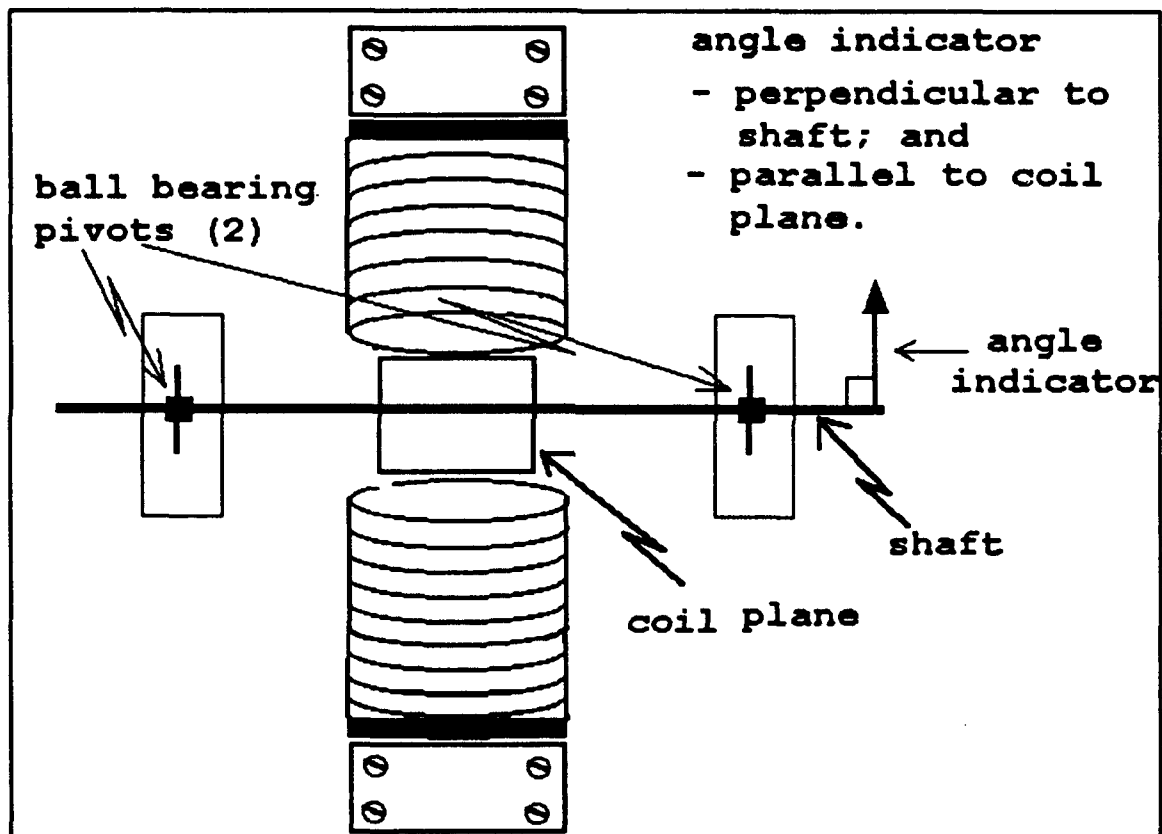


Figure 20. Angle indicator relative position.

The measurement of the center coil rotation angle is achieved using a small rod which extends perpendicular to the shaft holding the center coil, and parallel to the coil plane. This rod is

attached to the shaft and will rotate as a torque is applied to the center coil. This rod is referred to as the angle indicator (Figure 20). The rotation angle of center coil is obtained by measuring the vertical displacement of the angle indicator's edge (Figure 21), and the following relation:

$$\theta_{rot} = \sin^{-1} \left( \frac{y}{h} \right) \quad (46)$$

where

$h$  = the length of the angle indicator = 16.19 cm; and

$y$  = the vertical displacement of the angle indicator's edge from the rest position to the final position.

4.2.6 Static Imbalance. The mass distribution is unlikely to be uniform around the rotation axis. This results in a statically imbalanced system. The mass distribution around the rotation axis may be viewed as two masses of uniform density separated by an imaginary plane parallel to both the gravitational field and the rotation axis, and intersecting the rotation axis (Figure 22). A static imbalance is observed when the mass on either side of the plane is not equal. Consequently, the gravitational force on one side of the rotation axis is different than the gravitational force acting on the other side of the axis. Therefore, the center coil will rotate when the difference in gravitational force is greater than the friction. It will stop when the coil reaches a position where the difference of the gravitational force acting on either side of the imaginary plane is less than the friction. Accordingly,

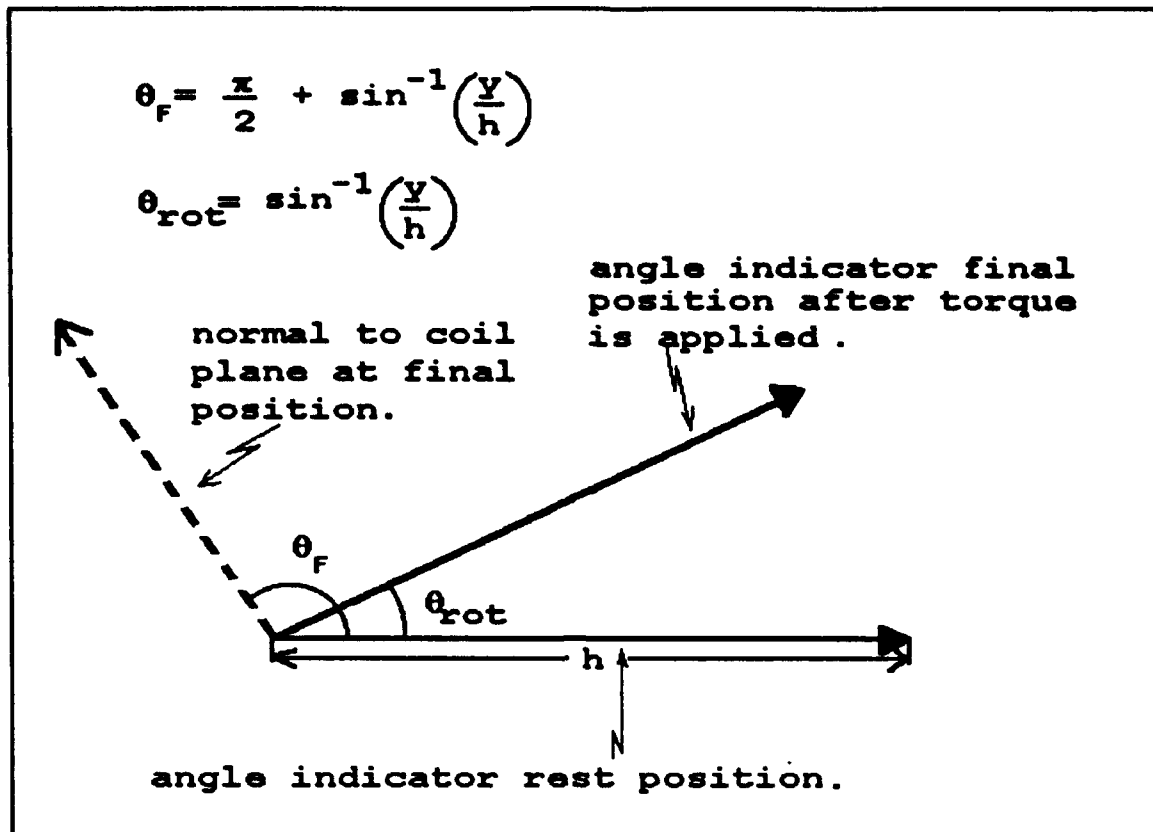


Figure 21. Definition of  $\theta_F$  and  $\theta_{rot}$ .

the aim is to reduce the static imbalance due to gravity to a magnitude less than the friction over the range of motion the center coil is expected to perform during the experiment.

The center coil rotation is in a 2 dimension space, the third dimension is restricted by the shaft holding the center coil. A uniform mass distribution is achieved by adding masses along the two axis which define the plane normal to the rotation axis (Figure 23). To verify that the mass distribution is uniform around the axis we simply positioned the angle indicator to a number of different angles at which the coil plane is expected to move during the experiment,  $0^\circ$ ,  $15^\circ$ ,  $30^\circ$ , ...,  $90^\circ$ . The system is considered

plane parallel to intersecting rotation axis, and  $\perp$  to earth's surface

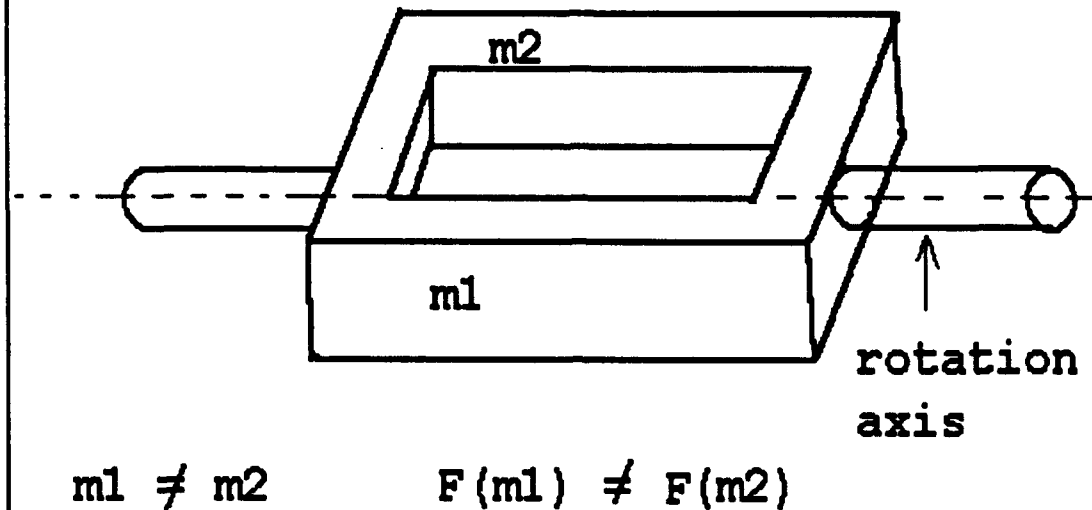


Figure 22. Center coil mass distribution.

balanced when the center coil does not rotate at any of the angles. As indicated earlier, if an imbalance exists the coil will rotate.

4.2.7 Test Setup. The dimensions and material details are included in Table IV. Using equation (3), (11) and (41) and the dimensions of the material, we estimated the maximum torque to be approximately 0.07 (N\*m). To obtain the maximum observable torque, friction must be kept to a minimum. Accordingly, the rod holding the center coil is mounted on bearings so that it may rotate as freely as possible as indicated in Figure 20.

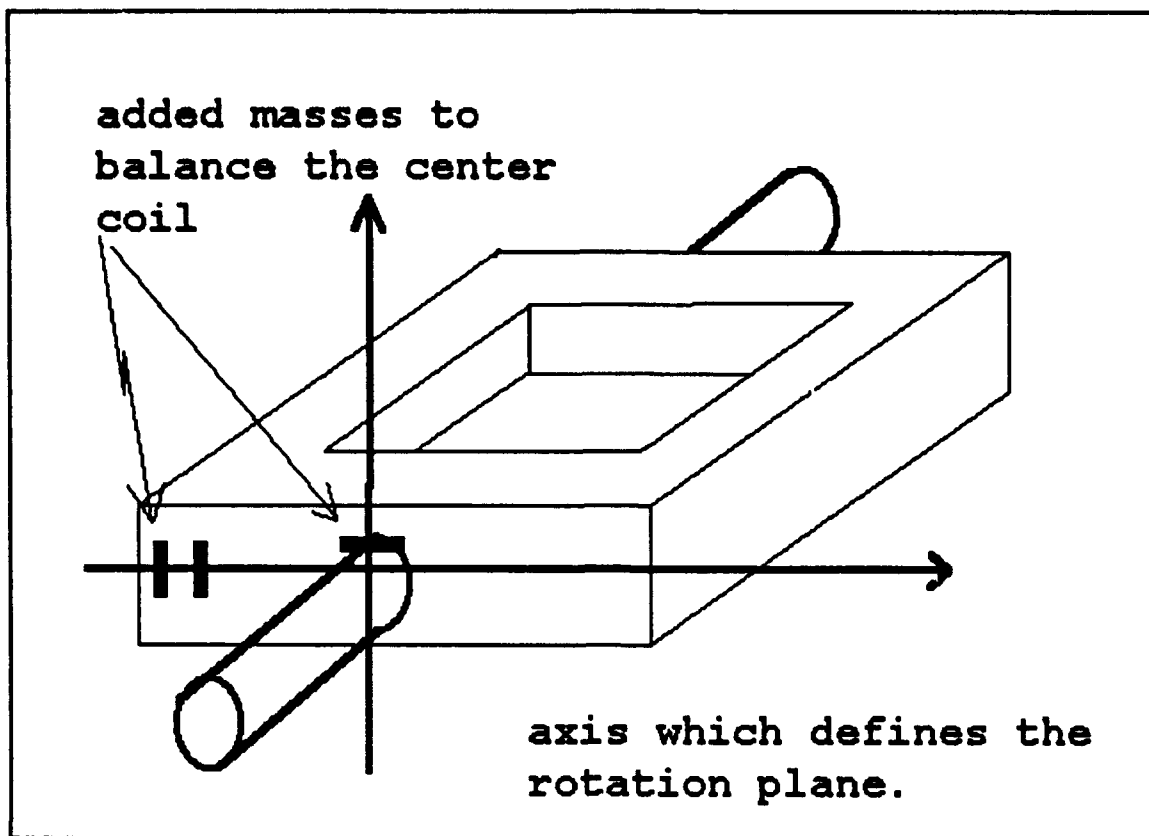


Figure 23. Balancing the center coil.

The initial dimension of the center coil did not provide a sufficient length to diameter ratio of the shield. As a result, the shield efficiency was affected and the rotation angle was reduced by a relatively low factor, 5. Therefore, the loop dimension was modified to 35 cm X 10 cm, which seemed to significantly improve the shielding efficiency as the rotation angle was reduced by a factor of 80 due to the presence of the shield. This new coil was not entirely exposed to the magnetic field since the diameter of the Helmholtz coils is 31 (cm). Therefore, the area of the coil exposed to the magnetic field was approximately 31 (cm) X 10 (cm). The remaining area of the loop was exposed to a non-linear magnetic field. This field is expected to decrease in intensity as the

**Table IV. Test hardware specifications.**

---

Helmholtz coil

length	0.94 (m)
radius	15.5 (cm)
wire size	AWG 24
No. turns	825
current	690 (mAmp)

Note: the distance between the two Helmholtz coils = 13.3 (cm)

Center Coil

Initial

length	20 (cm)
width	20 (cm)
wire size	AWG 24
No. turns	1000
current	700 (mAmp)
estimated torque	0.093 (N*m)

Modified

length	35 (cm)
width	10 (cm)
estimated torque	0.090 (N*m)

Shield

inside diam.	8.246 (cm)
outside diam	8.5 (cm)
thickness	0.0254 (cm)
# layers	10

---

distance from the Helmholtz coil increases. As discussed earlier the precise description of the magnetic field is not critical to the



experiment, as long as it is maintained constant throughout the experiment.

4.2.8 Limitation. The experiment design will demonstrate a limited shielded force ratio. As indicated at equation (45), the shielded force ratio is proportional to  $\sin(\theta_{F-shield}) / \sin(\theta_{F-unsh})$ . Accordingly, the maximum value of this ratio is limited to the maximum rotation angle which in turn is limited by the experiment design. For example, consider that the maximum rotation angle observed for an experiment is 60 degrees, that is  $\theta_{F-unsh} = 150$  degrees. Also, consider that the force is completely shielded, that is  $\theta_{F-shield} = 90$  degrees, that is the shielded coil experienced no rotation. Therefore, for this scenario the SFR is:

$$\frac{\sin(90^\circ)}{\sin(150^\circ)} = 2 \quad (47)$$

However, the force is entirely shielded which suggests that the shield efficiency is equal to infinity. This nonlinear relation between the SFR and the shield efficiency is due to the fact that friction is used as the basis for comparison between the shielded and unshielded induced force. In particular, the fact that the friction and the maximum torque are comparable in magnitude limits the SFR to a low ratio compare to the shield efficiency. On the other hand, if the torque was much greater than the friction, the SFR will tend towards infinity while the shield efficiency is significantly less. This is the case when the maximum rotation angle of the unshielded coil is  $90^\circ$ , that is  $\theta_{F-unsh} = 180^\circ$  making the denominator of equation (45) 0, and consider that  $\theta_{F-shield} = 170^\circ$ .

Consequently, the SFR becomes infinity while the shield efficiency is clearly less than infinity. Accordingly, the shield efficiency cannot be measure accurately due to the experimental design.

The aim of the experiment is to visually observe a significant reduction of the induced magnetic force in the presence of a magnetic shield. Accordingly, in the results section the data is presented in a format which support the aim of the experiment. In particular, it provides the rotation angle for the unshielded coil the shielded coil, and the shielded force ratio.

#### 4.3 Test Procedure

4.3.1 Unshielded Loop. The test procedure for this part of the experiment is relatively simple. Once the setup is completed, the Helmholtz coils and the center coil are independently connected to a power supply. The coil plane is initially positioned parallel to the magnetic field generated by the Helmholtz coil, and as the current circulates, the center coil will experience a torque which will tend to rotate the center coil to a position perpendicular to the magnetic field.

During this test procedure we found that the power source available was unable to provide the necessary current to reproduce the magnetic field ratio to which the shield will be exposed in a space environment. More specifically we intended to generate an  $H_{ext}$  10 times greater then the earth's magnetic field, and generate a current of 2 amps in a center coil made of 1000 turns. This scenario would have produced a field ratio of 60. However, the power supplies were only capable of producing a maximum of 0.700 amp

in the center coil. This decreased the torque to an unacceptable level, and, the  $H_{eff}$  was increased to approximately 100 times the magnitude of the earth's magnetic field to boost the torque to an acceptable level. Consequently, the field ratio for the experiment was approximately 2.

4.3.2 Shielded Loop. The second test procedure consisted of shielding the two segments of the loop on which an induced magnetic force would produce the torque. The cylindrical shields were prepared as part of the test procedure; it required that sheets of shielding material be cut to the appropriate dimension and then wrapped around the appropriate segments of the loop. Finally, the shield was held together using tape.

As discussed in Chapter 3 the shield thickness is critical to the shield efficiency; to achieve the appropriate thickness the foil is wrapped around the conductor until the accumulation of shield reaches the required thickness. The recommended procedure for joining part of the shield is to either use a "U" type joint or to simply weld the material together. Due to time and resource constraints these two techniques proved to be impractical, therefore, the joint were simply taped together. This procedure is taken into account when discussing the results.

Early in the test procedure we observed the significance of the end effect. The initial coil segments were 20 cm in length and the outside diameter of the shield was approximately 8.5 cm, as predicted for a length to diameter ratio of 2.33 the shield efficiency was significantly decreased. Therefore, the center coil

was rebuilt as to offer segments of 35 cm, thereby improving the length to diameter ratio to 4.17. Also, end caps were installed at the end of each cylinder.

4.3.3 Manual Shaking Procedure. As forecasted by the theoretical model, the shield becomes magnetized as the triggering magnetic fields are applied, removed and re-applied. Accordingly, an unplanned procedure had to be developed in order to demagnetize the shield. Based on the principle discussed for the shaking coil technique, the shield is manually demagnetized, after the magnetic fields are removed, by reversing the polarity of the external triggering field and rocking the shield  $180^\circ$  in this new field.

#### 4.4 Results.

The  $\theta_{rot}$  and the SFR were used as the basis to visually evaluate the ability to significantly reduce the induced magnetic force. The results are contained in Table V. With the rudimentary setup utilized in laboratory, it was clearly visible that the magnetic force was indeed reduced. We observed that the rotation angle was approximately 80 times smaller in the presence of a magnetic shield. Also, cylindrical shield end effects and magnetization of the shield were observed. The end effects were somewhat controlled by increasing the length of cylinder while maintaining the diameter constant and by installing end caps. Due to experimental design limitations it was impossible to precisely quantify the actual shield efficiency.

Table V. Measurements.

	Center Coil	$\theta_{\text{rot-unshi}}$ (rads)	$\theta_{\text{rot-shield}}$ (rads)	SFR
1st Application of triggering field	20 (cm) x 20 (cm)	1.083	0.180	2.100
16th Application of triggering field	20 (cm) x 20 (cm)	1.083	0.853	1.404
1st Application of triggering field	35 (cm) x 10 (cm)	0.730	0.009	1.340
11th Application of triggering field	35 (cm) x 10 (cm)	0.730	0.062	1.339
16th Application of triggering field	35 (cm) x 10 (cm)	0.730	0.123	1.330

The applied magnetic field within the shield is significantly less than the saturation field. Accordingly, the residual field was undetectable at first. However as the triggering fields were removed and reapplied a number of times, the cumulative effect of the residual field was observed as a significant decrease of the shields performance. Shield demagnetization was achieved by manually shaking the shield.

Finally, due to equipment limitations it proved impossible to obtain the magnetic field ratio to which the magnetic shield will be submitted to in space. This is not considered a significant drawback to this experiment. Indeed, as the theoretical model

suggest, it is more difficult to shield a 30 Oersted magnetic field than a 0.3 Oersted magnetic field.

#### 4.5 Conclusion

This experiment provided visual evidence that the induced magnetic force may be significantly reduced. Furthermore, the detection of the secondary effects such as magnetization and end effects, as predicted by the theoretical model, made the experiment more valuable in terms of supporting the feasibility study of the SCEP. Therefore, this experiment is considered a success.

## V. Conclusions and Recommendations

### 5.1 Conclusions

The aim of this study was to demonstrate the feasibility of using the interaction between the earth's magnetic field and a partly shielded coil structurally attached to the spacecraft to obtain a thrust. At the center of this study was a discussion on the ability to limit the force on the shielded segments of the loop and the shield itself. The theory indicates that the induced magnetic force depends on the velocity of the charge upon which the force is induced. Therefore, a change from a constant direction velocity, such as in the case of a current in a conductor wire, to a circular motion, such as in the case of an electron's spin, will modify the result of the interaction from a net force exerted on the conductor to a torque applied to the electron's spin within the shield. Finally, the domains of electron's spin are randomly oriented. Also, these electron's spin experience a torque when exposed to a magnetic field. Therefore, it may be concluded that the sum of all torques will be zero. The re-orientation of the spins will result in a surface magnetic current density. The magnitude of this current may be obtained using Laplace and Poisson's equations. As shown, these currents are quite small compared to the current being shielded.

Also, a review of the boundary conditions between the vacuum and the magnetic shield indicates that a magnetic field near a shield will be attracted and will have a tendency to remain trapped within the shield. This behavior associated with a cylindrical geometry explains why the external triggering magnetic field will be mostly deviated from the shielded region. Indeed, a portion of the magnetic field will penetrate through the shield into the shielded region. However, the amount of leakage is inversely proportional to the relative permeability of the shield. Since magnetic shields have very high relative permeability it is expected that the portion of the field which will penetrate the shielded region will be extremely small compared to an unshielded region. The shield may become saturated when exposed to a triggering field large enough that all domains within the shield have been re-oriented. Saturation of a shield is characterized by a sharp decrease of the relative permeability.

Therefore, there are three means by which magnetic force may be induced on a shielded conductor:

1. the internal triggering field will create a surface magnetic density current on the surface of the shield. The surface current on the outer surface may interact with the external triggering field, thereby possibly resulting in a net force;
2. the external triggering field will also create a surface magnetic current on the surface of the shield. The surface current on the inner surface will generate its own magnetic



field which may interact with the current carrying conductor and possibly result in a force; and

3. the small portion of the magnetic field which penetrates the shield in a direction almost normal to its surface and successfully penetrates the shielded region and induces a magnetic force on the shielded conductor.

For the three cases we were able to demonstrate that the magnitude of the forces that may be created is significantly smaller than the force induced on an unshielded current carrying conductor.

Finally, an experiment was conducted to support the theoretical findings. The experiment proved to be a success as it provided visual evidence that the induced magnetic force was significantly reduced by approximately 50% in the presence of a magnetic shield. Secondary effects such as end effects and shield magnetization were also observed, thereby providing additional evidence that the theoretical model is correct.

In order to provide some perspective on the actual potential of SCEP it may prove valuable to briefly highlight its advantages. The most significant particularity of this propulsion concept is that no propellant is necessary, thereby providing an extremely long lifetime. Also, the technology and materials required to construct the SCEP are available, inexpensive, and simple which in turn would make the system extremely reliable for space application.

## 5.2 Recommendations

5.2.1 Additional Validation - Model. This study centered on the force induced on a shielded conductor subjected to two

triggering fields. The shield is at rest with respect to the triggering fields. However, in low earth orbit the shielded conductor will be moving relative to the earth's magnetic field. The consequences of a relative motion between the external triggering field and the shield have not been addressed in this study. Therefore, further study is required to describe the behavior of the magnetic field in and around a magnetic shield moving relatively to the external triggering field.

Theoretical study is also required to further understand the magnetic shield process. In particular, the process of storing energy in the spin axis re-orientation could be quantified. This would allow the description of the shield as an energy storing device. Also, the laws of conservation of energy and angular momentum have not been verified, and, it should be part of future study.

In this study we considered a simple geometry shield which allowed us to described the magnetic field using closed form analytical expressions. More complex geometry, for which current expressions do not hold, will be required for future application. Therefore, numerical analysis techniques are required to evaluate the magnetic field behavior in and around a magnetic shield of more complex geometry. These techniques may have to be developed.

5.2.2 Application Considerations. The SCEP may at best offer 5 axis controls since it is not able to produce a force in the direction of the magnetic field. However, the theoretical study indicates that the magnetic field may vary in intensity and

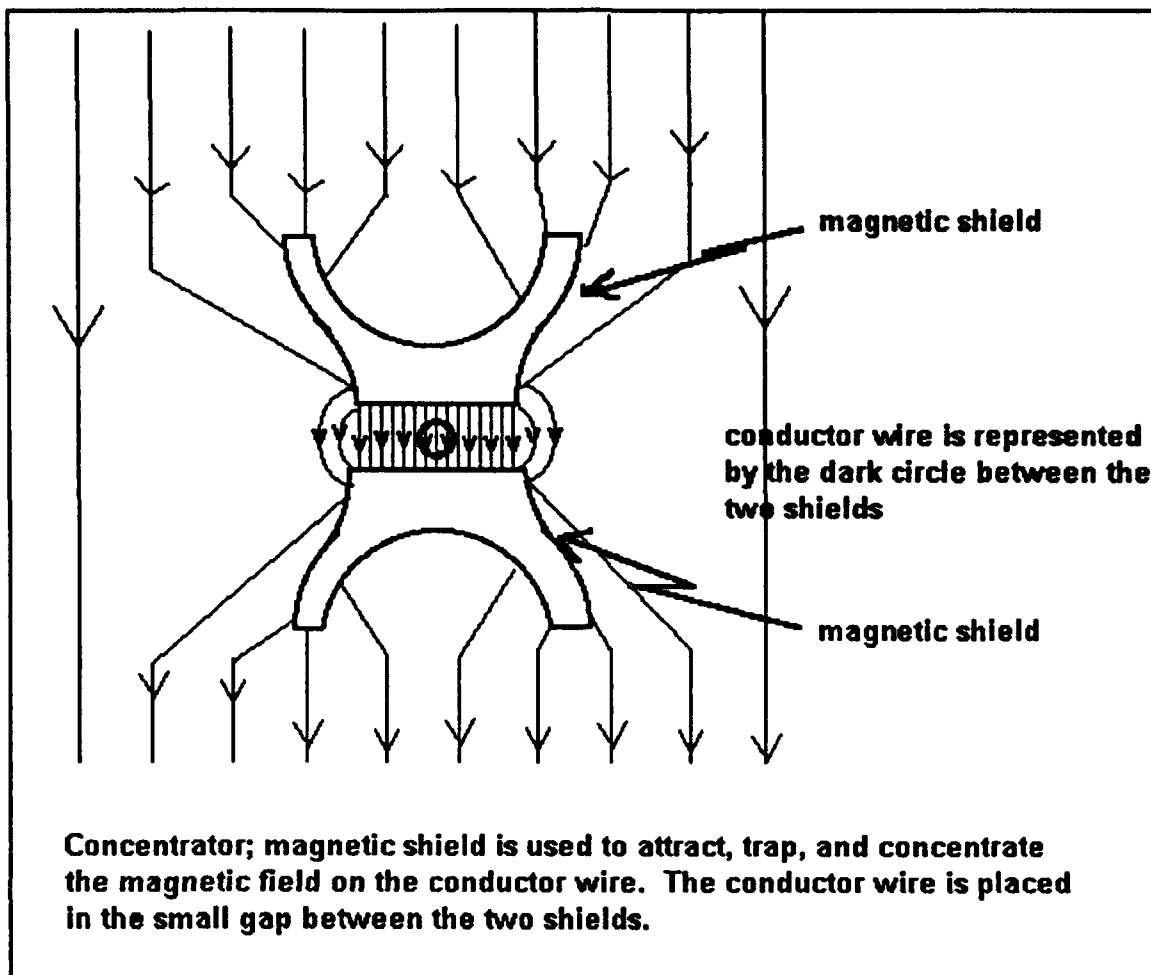


**Figure 24. Concentrator.**

direction around and within the magnetic shield. Therefore, uses could be made of these characteristics to improve the SCEP's performance. For example, the shield could be used as a concentrator (Figure 23). In this new configuration the problem becomes similar to the small gap toroid problem.

For the purpose of this thesis we simply demonstrated the feasibility of SCEP. At this point it would be appropriate to define specific mission requirements and optimize the design of the SCEP to satisfy those requirements. For example, the mission may

be to provide LEO to GEO orbit transfer in a period of less than 10 days. Accordingly, the dimensions of the conductors and power source would be designed to satisfy that mission. In particular, the SCEP may operate on high intensity short duration power impulse, therefore, it may prove profitable to use capacitors in lieu of batteries.

An overall optimization study should be considered in order to define better propulsion components. For example, other conducting material such as a conducting polymer may be used instead of an aluminum conductor in order to reduce the weight of the propulsion system.

Control issues will also have to be addressed. In particular, the current level to be provided to the different loops will vary with the task and the relative position of the earth's magnetic field. Also, the shield efficiency will vary as a function of the current level. Therefore, a controlling device which will take into consideration these factors will have to be developed.

The SCEP is a very promising space propulsion concept. It has the potential to develop into space application beyond current system capability.

## Appendix A: Magnetic Field - Internal Triggering Field

The purpose of this appendix is to provide a closed form analytical expression for the magnetic field generated by a current carrying conductor positioned along the axis of cylindrical shield. A cylindrical coordinate reference system with the  $z$  axis defined by the conductor wire is used to describe the magnetic field (Figure 25).

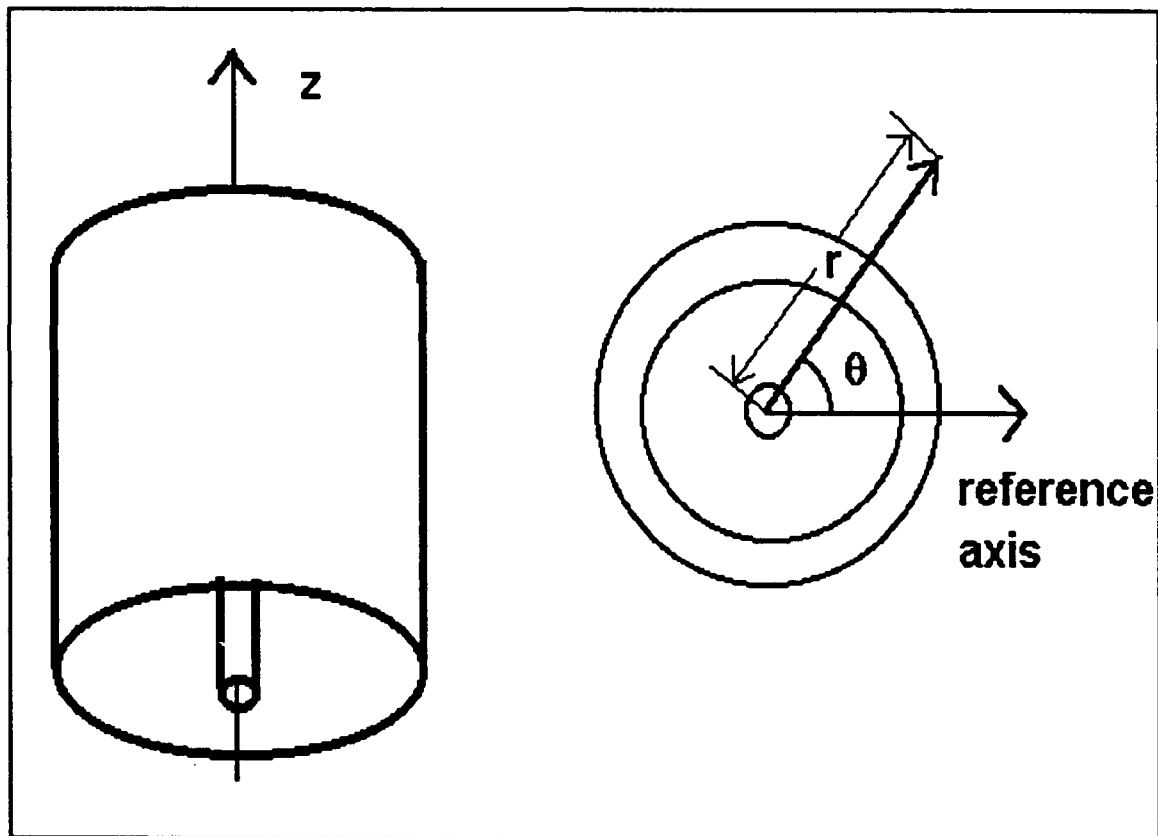


Figure 25. Cylindrical coordinate reference system.

A number of assumptions are made in order to simplify the analysis of the problem. The first assumption will be that the

conductor wire and the shield are infinitely long. This assumption is considered valid when two conditions are satisfied:

1. The distance "r" at which the magnetic field is described is at least 10 times smaller than the conductor wire's length;
2. The distance from the conductor ends at which the magnetic field is described is at least 10 times greater than "r".

The second assumption is that the surface magnetic current density created on the outer surface of the magnetic shield ( $J_{sm-out}$ ) is equal and opposite in direction to the surface magnetic current density created on the inner surface of the shield ( $J_{sm-in}$ ). As discussed in Chapter 2, the magnetic surface current density results from the re-orientation of the electron spin magnetic moment. The number of re-oriented magnetic moment which created  $J_{sm-out}$  is equal to the number of re-oriented magnetic moment which created  $J_{sm-in}$ . The outer shield diameter is obviously larger than the inner diameter. Therefore,  $J_{sm-out}$  will be smaller than  $J_{sm-in}$ , the ratio may be derived and is given by:

$$\frac{J_{sm-in}}{J_{sm-out}} = \frac{D_{out}}{D_{in}} \quad (48)$$

The diameter of the shield is typically 100 times greater than the thickness of the shield. Accordingly, the ratio in equation (48) is typically 1.02, and  $J_{sm-out}$  is approximately equal to  $J_{sm-in}$ .

This assumption allows us to compare the applied magnetic field created by the surface magnetic current density to the magnetic field created inside a solenoid. In particular the magnetic field

inside an infinitely long solenoid is constant (Johnk, 1975:42). Therefore, the applied magnetic field will be assumed constant throughout the shield. Consequently, it may also be assumed that the relative permeability will be constant within the shield.

The potential function  $\Phi$  in cylindrical coordinate reference system is used to define the magnetic field in and around the shield. The relation between the magnetic field and the potential function is given by (Van Bladel, 1964:163):

$$H(r,\theta) = -[\hat{u}_z \times \nabla \Phi(r,\theta)] \quad (49)$$

where  $\hat{u}_z$  = the unit vector along the z axis in the cylindrical coordinate reference system. From this expression it may be concluded that the magnetic field is independent of the position along the z axis. Therefore, the magnetic field may be described in a two dimension space, and the potential function may be defined using two variable, "r" and " $\theta$ ".

Consider the field created outside a current carrying conductor in an isotropic and homogeneous medium (i.e. absence of magnetic shield). The expression of the potential function associated with the field is given by:

$$\Phi_{in}(r) = \frac{-J_{wire} \rho_{wire}^2 \ln(r)}{2} \quad (50)$$

where:

$\rho_{wire}$  = is the radius of the conductor wire(m);

$r$  = the distance from the conductor wire(m); and

$J_{\text{wire}}$  = current density due to current in the wire (amp/m<sup>2</sup>).

The validity of equation (50) may be verified using equation (49). The medium is then modified by the insertion of a high permeability cylinder around the conductor wire. As discussed in Chapter 2, a magnetic surface current density will be created at the surface of the shield. This surface current density will in turn create a magnetic field. The magnetic field within a uniform current density equal zero (Krauss, 1984:171). As a result of the initial assumptions, that is an isotropic and homogeneous medium, and a constant relative permeability, the magnetic surface current density may be considered uniform. Accordingly, the magnetic field created by the magnetic surface current density will equal zero inside of the cylinder. Therefore, equation (50) remains valid over the region limited by the inside diameter of the shield and the outside diameter of the conductor wire.

To define the magnetic field outside and within the shield we now consider Laplace's equation:

$$\nabla^2 \Phi = 0 \quad (51)$$

The form of the general solution to Laplace's equation in a two dimension space is given by:

$$\Phi(r,\theta) = (A r + C /r)\sin(\theta) + (D r + E /r) \cos(\theta) \quad (52)$$



This equation represents the potential function of a magnetic field in an isotropic and homogeneous medium. Accordingly, we shall define the potential within the magnetic shield as:

$$\begin{aligned}\Phi_{shield}(r,\theta) = & (A_{shield} r + C_{shield} /r) \sin(\theta) \\ & + (D_{shield} r + E_{shield} /r) \cos(\theta)\end{aligned}\tag{53}$$

and the potential outside the shield as:

$$\begin{aligned}\Phi_{out}(r,\theta) = & (A_{out} r + C_{out} /r) \sin(\theta) \\ & + (D_{out} r + E_{out} /r) \cos(\theta)\end{aligned}\tag{54}$$

One more condition applies to the magnetic field outside the shield. Since the magnetic field at infinity tends to zero, the potential function must be defined at infinity. Therefore, the value of the constants  $A_{out}$  and  $D_{out}$  must be zero. The equation for the potential function outside the shield may be rewritten as:

$$\Phi_{out}(r,\theta) = C_{out} /r \sin(\theta) + E_{out} /r \cos(\theta)\tag{55}$$

The problem then becomes one of determining the value of the constant  $A_{shield}$ ,  $C_{shield}$ ,  $D_{shield}$ ,  $E_{shield}$ ,  $C_{out}$ ,  $E_{out}$ . We apply the boundary conditions, which are given by (Krauss, 1984: 238):

$$\mu_{r-out} \frac{\partial \phi_{out}}{\partial r} = \mu_{r-shield} \frac{\partial \phi_{shield}}{\partial r} \quad (56)$$

and

$$\frac{1}{r} \frac{\partial \phi_{shield}}{\partial \theta} - \frac{1}{r} \frac{\partial \phi_{out}}{\partial \theta} = J_{sm} \quad (57)$$

where  $\mu_{r-out} = 1$  since it is the vacuum.

Two boundaries are define for this problem:

1. one boundary defines the transition from the shielded region (vacuum) to within the shield. This boundary is at a distance  $r = a$ ; and
2. the other boundary defines the transition from within the shield to outside of the shield (vacuum). This boundary is at a distance  $r = b$  from the center of the conductor wire.

At  $r = a$ , the first boundary conditions gives:

$$\begin{aligned} &\mu_{r-shield} (A_{shield} - C_{shield} / b^2) \sin(\theta) + \\ &\mu_{r-shield} (D_{shield} - E_{shield} / b^2) \cos(\theta)) = \\ &- C_{out} / b^2 \sin(\theta) - E_{out} / b^2 \cos(\theta) \end{aligned} \quad (58)$$

and the second boundary condition gives:

$$\begin{aligned}
& (A_{shield} + C_{shield} / b^2) \cos(\theta) - \\
& (D_{shield} + E_{shield} / b^2) \sin(\theta)) - \\
& - C_{out} / b^2 \cos(\theta) + E_{out} / b^2 \sin(\theta) = J_{sm}
\end{aligned} \tag{59}$$

These equations are valid at any angle, therefore, they must be at valid at  $\theta = \pi/2$  and at  $\theta = 0^\circ$ . Accordingly, at  $\theta = \pi/2$  equation (58) becomes:

$$\mu_{r-shield} (A_{shield} - C_{shield} / b^2) = - C_{out} / b^2 \tag{60}$$

and equation (59) becomes:

$$(D_{shield} + E_{shield} / b^2) - E_{out} / b^2 = -J_{sm} \tag{61}$$

at  $\theta = 0^\circ$  equation (58) becomes:

$$\mu_{r-shield} (D_{shield} - E_{shield} / b^2) = - E_{out} / b^2 \tag{62}$$

and equation (59) becomes:

$$-(A_{shield} + C_{shield} / b^2) + C_{out} / b^2 = -J_{sm} \tag{63}$$

the last four equations may rewritten as:

$$E_{shield} = \frac{E_{out}}{2} \left( \frac{1}{\mu_{r-shield}} + 1 \right) - \frac{J_{sm} b^2}{2} \tag{64}$$

$$D_{shield} = -\frac{J_{sm}}{2} + \frac{E_{out}}{2 b^2} \left( 1 - \frac{1}{\mu_{r-shield}} \right) \quad (65)$$

$$C_{shield} = \frac{C_{out}}{2} \left( \frac{1}{\mu_{r-shield}} + 1 \right) + \frac{J_{sm} b^2}{2} \quad (66)$$

$$A_{shield} = \frac{C_{out}}{2 b^2} \left( 1 - \frac{1}{\mu_{r-shield}} \right) + \frac{J_{sm}}{2} \quad (67)$$

Now we re-apply the boundary conditions at  $r = a$ . The first boundary condition yields:

$$\begin{aligned} \mu_{r-shield} (A_{shield} - C_{shield} / a^2) \sin(\theta) + \\ \mu_{r-shield} (D_{shield} - E_{shield} / a^2) \cos(\theta) = \\ -\frac{J_{wire} \rho_{wire}^2}{2 a} \end{aligned} \quad (68)$$

and the second condition yields:

$$\begin{aligned}
 & -(A_{shield} + C_{shield} / a^2) \cos(\theta) + \\
 & (D_{shield} + E_{shield} / a^2) \sin(\theta) = J_{sm}
 \end{aligned} \tag{69}$$

at  $\theta = \pi/2$  and  $\theta = 0$  equations (68) and (69) becomes:

$$\mu_{r-shield} (A_{shield} - C_{shield} / a^2) = -\frac{J_{wire} \rho_{wire}^2}{2 a} \tag{70}$$

$$(D_{shield} + E_{shield} / a^2) = J_{sm} \tag{71}$$

$$\mu_{r-shield} (D_{shield} - E_{shield} / a^2) = -\frac{J_{wire} \rho_{wire}^2}{2 a} \tag{72}$$

$$(A_{shield} + C_{shield} / a^2) = -J_{sm} \tag{73}$$

These four equations combined yield the following four equations:

$$D_{shield} = \frac{J_{sm}}{2} - \frac{J_{wire} \rho_{wire}^2}{4 \mu_{r-shield} a} \tag{74}$$

$$A_{shield} = -\frac{J_{sm}}{2} - \frac{J_{wire} \rho_{wire}^2}{4 \mu_{r-shield} a} \tag{75}$$

$$C_{shield} = \frac{-J_{sm} a^2}{2} + \frac{J_{wire} \rho_{wire}^2 a}{4 \mu_{r-shield}} \quad (76)$$

$$E_{shield} = \frac{J_{sm} a^2}{2} - \frac{J_{wire} \rho_{wire}^2 a}{4 \mu_{r-shield}} \quad (77)$$

Combining equations (67) and (75) yields:

$$C_{out} = \left( -2 b^2 J_{sm} - \frac{b^2 J_{wire} \rho_{wire}^2}{2 \mu_{r-shield} a} \right) \frac{\mu_{r-shield}}{\mu_{r-shield} - 1} \quad (78)$$

Combining equations (66) and (76) yields:

$$C_{out} = \left( -J_{sm} (a^2 + b^2) + \frac{J_{wire} \rho_{wire}^2 a}{2 \mu_{r-shield}} \right) \frac{\mu_{r-shield}}{\mu_{r-shield} + 1} \quad (79)$$

Combining the last two equations:

$$J_{sm} = \frac{\frac{J_{wire} \rho_{wire}^2}{2 \mu_{r-shield}} \left( -\frac{b^2}{a (\mu_{r-shield} - 1)} - \frac{a}{(\mu_{r-shield} + 1)} \right)}{\frac{-a^2 - b^2}{\mu_{r-shield} + 1} + \frac{2 b^2}{\mu_{r-shield} - 1}} \quad (80)$$

Making the approximation that  $\mu_r \gg 1$ , the last equation may be rewritten as:

$$J_{sm} = -\frac{J_{wire} \rho_{wire}^2 (b^2 + a^2)}{2 \mu_{r-shield} a (b^2 - a^2)} \quad (81)$$

also,  $D_{in} = 2a$  and  $D_{out} = 2b$ , therefore the previous equation becomes:

$$J_{sm} = -\frac{J_{wire} \rho_{wire}^2 (D_{out}^2 + D_{in}^2)}{\mu_{r-shield} D_{in} (D_{out}^2 - D_{in}^2)} = \frac{H_{if} (D_{out}^2 + D_{in}^2)}{\mu_{r-shield} (D_{out}^2 - D_{in}^2)} \quad (82)$$

This is the solution to the magnetic surface current density at the surface of the magnetic shield. The negative sign indicates that the current at the outside boundary runs in an opposite direction to the current in the conductor wire. The other constants are determined by substitution of equation (81) into equations (65), (74), (75), (76), (77) and (78).

To determine the magnitude of the magnetic field within the shield, we use the following relation:

$$H_{app} = \frac{J_{sm}}{(\mu_r - 1)} \quad (83)$$

if the assumption that  $\mu_r \gg 1$  prevails, the magnetic field density within the shield will be:

$$B_{app} = \mu_0 J_{sm} = \mu_0 \frac{J_{wire} \rho_{wire}^2 (b^2 + a^2)}{2 a (b^2 - a^2)} \quad (84)$$

this expression may be rewritten in terms of the magnetic field created by a current carrying conductor, that is, the internal triggering field:

$$B_{app} = \mu_o H_{if} \frac{(b^2 + a^2)}{(b^2 - a^2)} \quad (85)$$

and, this equation may also be rewritten in terms of the inside and outside diameter of the shield:

$$B_{app} = \mu_o H_{if} \frac{(D_{out}^2 + D_{in}^2)}{(D_{out}^2 - D_{in}^2)} \quad (86)$$



## Bibliography

- Baum, E. and Bork, J. "Systematic design of magnetic shields," Journal of Magnetism and Magnetic Materials, 101 : 69 -74 (1991).
- Bladel, J. Van Electromagnetic Fields. New York: McGraw-Hill Book Company, 1964.
- Drell, S.D. and others. "Drag and Propulsion of Large Satellites in the Ionosphere An Alfven Propulsion Engine in Space," Journal of Geophysical Research, Vol. 70, No. 13, 3131-3145, July 1965.
- Engelberger, J,F. "Space Propulsion System." United States Patent Office, patent no 3,504,868, patented 7 Apr 1970.
- Fink, Donald G. and Carroll, John M. Standard Handbook for Electrical Engineers (Tenth Edition). New York: McGraw Hill Book Company, 1968.
- Haga, A. and Nasuno, H. "Characteristics and Application of C-Shaped Magnetic Sheets," IEEE Translation Journal on Magnetic in Japan, 5: 755-761 (1990).
- Heisenberg, W. On the theory of ferromagnetism. Zeit. f. Phys., 1928.
- Hyat, William Hart Engineering Electromagnetic. New York: McGraw-Hill Book Company, 1974.
- Janson, S.W. "The On-Orbit Role of Electric Propulsion," AIAA/SAE/ASME/ASEE 29th Joint Propulsion Conference and Exhibit. 1-13. Monterey, CA: AIAA 93-2220, 1993

Johnk, Carl T. A. Engineering Electromagnetic Fields and Waves.  
New York: John Wiley & Sons, 1975.

Krauss, John, D. Electromagnetic. New York: McGraw-Hill Book  
Company, 1984.

Lorrain, Paul and Corson, Dale, R. Electromagnetic Fields and  
Waves. San Francisco: W.H. Freeman and Company, 1970.

Lawrence, Richard E. Jr. An Electromagnetically-Controlled  
Precision Orbital Tracking Vehicle. MS thesis,  
AFIT/GA/ENY/92D-05. School of Engineering, Air Force  
Institute of Technology, Wright-Patterson AFB OH, December  
1992.

Mager, Albrectht J. "Magnetic Shields," IEEE Transactions on  
Magnetic, 6: 67-74 (March 1970).

Magnetic Shield Corp. Material and Fabrication Guide. Catalog MG-  
5F. Perfection Mica Company, 740 North Thomas Drive,  
Bensenville, Illinois 60106 U.S.A., 1991.

Magnetic Shield Corp. Magnetic Shielding Lab Kit with AC Probe.  
Catalog LK-2G. Perfection Mica Company, 740 North Thomas  
Drive, Bensenville, Illinois 60106 U.S.A., 1991.

Penzo, Paul A. and Ammann, Paul W. National Aeronautics and Space  
Administration. Tethers in Space Handbook (Second Edition).  
Contract Number: NASW-4341, May 1989.

Rikitake, Tsuneji. "Magnetic Shielding by a Spherical shell  
Having a Hole(1)," Journal of Geomagnetism and  
Goelectricity, 45: 1221-1235 (1990).

Spenny, C.H., and R.E. Lawrence Jr. "A Precision Orbital Tracking Vehicle (POTkV)," AIAA/SAE/ASME/ASEE 29th Joint Propulsion Conference and Exhibit. AIAA 93-2226 Montarey, CA: AIAA 993.

Sutton, George P. Rocket Propulsion Elements (Sixth Edition). New York: John Wiley & Sons, Inc, 1992.

Väino O. , R. Peltonen, and Börje Rantala. "The Effect of Shaking on Magnetic Shields," IEEE Transactions on Magnetic, 16: 575-578 (July 1980).

### Vita

Major Richard J.R. Ladouceur was born on 8 September 1960 in Saint-Eustache, Québec, Canada. He joined the Canadian Armed Forces in 1980 and received his commissioning scroll upon graduation from Air Navigation Training in 1982. He completed his first tour of duty with the 405 Maritime Patrol Squadron. In 1986 he attended the Collège Militaire Royal de Saint-Jean where he completed his undergraduate degree. In 1988 he returned to the 405 Squadron and was employed as the Tactical Cell Leader. He was promoted to his current rank in 1990 and was selected to serve as Promotion Policy officer at National Defence Headquarter. He remained in Ottawa until his affectation to AFIT in 1992.

Permanent address: 4949 Amberwood Dr.  
Dayton, Ohio 45424.

<b>REPORT DOCUMENTATION PAGE</b>			Form Approved OMB No. 0704-0188	
<small>When reporting burdens on this form, the information is estimated to average 1 hour per response, including the time for reviewing instructions, searching existing data sources, gathering and maintaining the data needed, and completing and reviewing the collection of information. Send comments regarding this burden estimate or any other aspect of this collection of information, including suggestions for reducing this burden, to Washington Headquarters Services, Directorate for Information Operations and Reports, 1215 Jefferson Davis Highway, Suite 1204, Arlington, VA 22202-4302, and to the Office of Management and Budget, Paperwork Reduction Project (0704-0188), Washington, DC 20503.</small>				
1. AGENCY USE ONLY (Leave blank)		2. REPORT DATE <b>DEC 93</b>	3. REPORT TYPE AND DATES COVERED <b>Master's Thesis</b>	
4. TITLE AND SUBTITLE <b>SHIELDED COIL ELECTRODYNAMIC PROPULSION (SCEP) - A FEASIBILITY STUDY</b>			5. FUNDING NUMBERS	
6. AUTHOR(S) <b>Maj Richard J.R. Ladouceur</b>				
7. PERFORMING ORGANIZATION NAME(S) AND ADDRESS(ES) <b>Air Force Institute of Technology, WPAFB OH 45433-6538</b>			8. PERFORMING ORGANIZATION REPORT NUMBER <b>AFIT/GSO/ENY/93D-6</b>	
9. SPONSORING / MONITORING AGENCY NAME(S) AND ADDRESS(ES) <b>N/A</b>			10. SPONSORING / MONITORING AGENCY REPORT NUMBER	
11. SUPPLEMENTARY NOTES				
12a. DISTRIBUTION / AVAILABILITY STATEMENT <b>Approved for public release; distribution unlimited</b>			12b. DISTRIBUTION CODE	
13. ABSTRACT (Maximum 200 words) <b>This study investigated Shielded Coil Electrodynamic Propulsion (SCEP). The use of the earth's magnetic field as a propulsion source has been previously investigated. It was found that a significant amount of power and long conductors were required. A more compact propulsion concept which requires significantly less power is proposed. This concept relies on the feasibility of significantly reducing the magnetic force induced by the earth's magnetic field on selected segments of a coil. An experiment design to support the theoretical findings was conducted. The experiment results support the theoretical model.</b>				
14. SUBJECT TERMS <b>magnetic shield, electrodynamic propulsion</b>			15. NUMBER OF PAGES <b>108</b>	
			16. PRICE CODE	
17. SECURITY CLASSIFICATION OF REPORT <b>Unclassified</b>	18. SECURITY CLASSIFICATION OF THIS PAGE <b>Unclassified</b>	19. SECURITY CLASSIFICATION OF ABSTRACT <b>Unclassified</b>	20. LIMITATION OF ABSTRACT <b>UL</b>	